T CELLS

FoxP3 associates with enhancer-promoter loops to regulate T_{reg}-specific gene expression

Ricardo N. Ramirez, Kaitavjeet Chowdhary, Juliette Leon, Diane Mathis*, Christophe Benoist*

Gene expression programs are specified by higher-order chromatin structure and enhancer-promoter loops (EPLs). T regulatory cell (T_{reg}) identity is dominantly specified by the transcription factor (TF) FoxP3, whose mechanism of action is unclear. We applied chromatin conformation capture with immunoprecipitation (HiChIP) in T_{reg} and closely related conventional $CD4^+$ T cells (T_{conv}). EPLs identified by H3K27Ac HiChIP showed a range of connection intensity, with some superconnected genes. TF-specific HiChIP showed that FoxP3 interacts with EPLs at a large number of genes, including some not differentially expressed in T_{reg} versus T_{conv}, but enriched at the core T_{reg} signature loci that it up-regulates. FoxP3 association correlated with heightened H3K27Ac looping, as ascertained by analysis of FoxP3-deficient T_{reg}-like cells. There was marked asymmetry in the loci where FoxP3 associated at the enhancer- or the promoter-side of EPLs, with enrichment for different transcriptional cofactors. FoxP3 EPL intensity distinguished gene clusters identified by single-cell ATAC-seq as covarying between individual T_{regs}, supporting a direct transactivation model for FoxP3 in determining T_{reg} identity.

INTRODUCTION

Looping is the solution that allows the packaging of the gigantic strands of chromosomal DNA into tight nuclear spaces while ensuring the spatial organization and connectivity essential for the orderly deployment of their coding capacity (*1*–*3*). Some of the resulting topologies are very large, on the greater than megabase scale, such as the higher-order compartment domains, and primarily relate to overall organization. More directly associated with the unfolding of the genome's coding potential are the enhancer-promoter loops (EPLs) that bring distal enhancers into close proximity to transcriptional start sites (TSSs) in the three-dimensional (3D) space, enabling their interactions to regulate transcriptional programs (*4*–*6*). Rewiring of EPLs occurs during differentiation in several mammalian systems, ranging from early differentiation to olfactory receptor allelic choice (*7*–*10*). It has been proposed (*5*) that programmatic shifts associated with differentiation involve new enhancer-promoter connectivity, whereas the fast responses to stimuli or growth factors exploit preexisting contacts, by modifying the activity of associated proteins (*11*–*13*). This dichotomy may not be as well defined as stated, and it is unclear how much EPL rewiring exists between closely related cells. Loops are dynamic structures, and the burst-like nature of transcriptional output may correspond to transient enhancer-promoter interactions (*14*). Last, how sequence-specific transcription factors (TFs) coopt the EPL landscape remains mostly hypothetical. Intuitively, fast-acting TFs whose mechanism of action relies on nuclear translocation (e.g., NF-AT) or activation at the cell membrane (e.g., STATs) likely operate on preexisting EPLs. Other TFs might, instead, provoke the formation of new EPLs by dimerization (*15*) or macromolecular complex formation. A corollary question is whether an EPL is intrinsically sufficient for transactivation or only a framework onto which activation mechanisms latch (*4*, *5*). The regulatory function of TFs operating via EPLs has been demonstrated for both cell-specific and general TFs (e.g., Klf4 and Yy1, respectively) (*16*, *17*).

Department of Immunology, Harvard Medical School, Boston, MA 02115, USA.
*Corresponding author. Email: cbdm@hms.harvard.edu

T regulatory cells (T_{regs}) are a branch of $CD4^+$ T cells that act as dominant negative regulators of many facets of the immune system (*18*, *19*). They also control extraimmunologic consequences of inflammation in several organs (*20*). Consistent with these pleiotropic functions, several phenotypic variants of $FoxP3^+$ T_{regs} exist, with tuned transcriptomes that adapt to their tissue localization and effector functions (*21*). FoxP3, a member of the forkhead/winged-helix family of TFs, is quasi-exclusively expressed in T_{regs} and plays a central role in determining their identity and function and their characteristic transcriptional signature. It is, however, neither completely necessary nor sufficient for T_{reg} determinism (*22*–*25*) and requires synergistic action from a number of transcriptional cofactors with which it interacts (*26*–*31*). FoxP3 is not a pioneer factor, as many of the enhancers and open chromatin regions (OCRs) to which it binds are already accessible in the T cell lineage before FoxP3 expression (*32*, *33*), although a smaller group of FoxP3-binding OCRs are activated contemporaneously with T_{reg} differentiation.

While FoxP3 can synergize with several sequence-specific TFs and with chromatin modifiers, its true mechanism of action remains poorly understood. There is debate as to it being an activator or a repressor and even whether it activates T_{reg}-specific transcription directly or by tuning intermediates. Some have argued that it functions primarily as a transcriptional repressor (*26*, *27*, *34*–*36*). The repression of cytokines produced upon activation by conventional $CD4^+$ T cells (T_{conv}), and, in particular, interleukin-2 is a well-established function of FoxP3. Conversely, results from several experimental systems suggest that FoxP3 also behaves as an activator for many of its transcriptional targets (*31*, *37*–*40*) and that this is its principal mode of action. The "cofactor model" posits that this functional dichotomy depends on the identity of the cofactor(s) with which it interacts in controlling specific targets (*27*, *31*, *38*). Superresolution microscopy does show FoxP3 associated with activating or repressive cofactors in different "transcriptional hubs" in the nucleus of the same T_{reg} (*31*).

An important missing piece of the FoxP3 puzzle is an understanding of its interactions with nuclear loop structures, particularly enhancer-promoter connectivity. Chromatin immunoprecipitation

sequencing (ChIP-seq) data show FoxP3 binding in the vicinity of TSS and at distant enhancers (*31*, *32*, *41*), but how FoxP3 interrelates with EP connectivity is unknown. Does FoxP3 enhance or disrupt the formation of specific EPLs in T_{regs}? Does it dock onto existing loop structures to nucleate regulatory (activating or inhibitory) complexes? Here, we examine this question by using chromatin conformation capture with immunoprecipitation (HiChIP), first with anti-H3K27Ac antibody to establish the comparative landscape of EPLs in primary T_{reg} and T_{conv} cells, two closely related cell types. We then map FoxP3 molecules onto T_{reg} EPLs. Directly relevant to the question of FoxP3 mechanics, the results show that FoxP3-bearing EPLs correspond to strong H3K27Ac loops genome wide and positively associate with differential transcription between T_{conv} and T_{regs}, consistent with action as a direct transcriptional activator.

RESULTS

Mapping the enhancer-promoter connectome in T_{reg} and T_{conv} cells

To understand how the short- and long-range enhancer-promoter contacts mediate the cell type–specific expression patterns among mouse $CD4^+$ T cells, we first used the HiChIP method (*9*), which identifies chromatin loops associated with a histone mark or a particular TF by combining proximity ligation of DNA strands with immunoprecipitation, quantitated by high-throughput sequencing. Antibodies against H3K27Ac, the histone modification typical of active enhancers, focused the analysis on loops connecting active enhancers. We analyzed primary mouse T_{reg} and T_{conv} cells directly purified ex vivo to avoid imprints from cell culture, aiming for deep libraries to support robust quantitative analysis (200 to 300 M reads per sample on average; table S1). This required sizeable numbers of cells, achieved by magnetic purification from *Foxp3-Thy1.1* reporter mice. In line with current practice (*42*, *43*), we quantitated EPL signals as reads that connect the promoter region (±500 bp around the TSS) to 5-kb bins tiled ±250 kb from the gene's TSS. To correct for proximity-biased background in HiChIP data, we compared the EPL signals to a null distribution generated from the interactions of 1000 random intragenic positions, which allowed estimates of significance corrected for relative distance to the TSS [similar to (*42*–*44*)]. Signals were conserved among biological replicates (fig. S1A). A control HiChIP with an irrelevant isotype-matched antibody showed that the vast majority of H3K27Ac+ EPLs were specific ($P < 0.0001$; fig. S1B).

Across both T_{reg} and T_{conv}, 115,538 significant EPLs were identified [false discovery rate (FDR) of 0.05] among 9058 genes selected for reliable mRNA expression in T_{reg} or T_{conv} cells (data file S1), as illustrated for *Lrrc32* (Fig. 1A). The median H3K27Ac EPL size was 49.5 kb (fig. S1C), concordant with EPL size estimates in other mammalian cells (*7*, *9*). Only 0.5% of H3K27Ac EPLs reached further than 1 Mb from the TSS, indicating that such very long range interactions can occur but are the exception. Cumulative EPL intensity for each gene was only marginally related to its mRNA levels (fig. S1D), fitting with recent reports (*5*, *45*).

A gene's cumulative EPL intensity showed a linear relationship to its number of EPLs (Fig. 1B). At first blush, this is mathematically obvious, but on further thought, it implies that an active promoter does not simply allocate a fixed interaction potential by alternating between its potential enhancers. Each enhancer has a given probability of interaction, and these are cumulated for each gene (plausibly by corecruitment into a transcriptional hub). This continuity suggests that the regulatory cross-talk of enhancers that loop to the same promoter operates through additive modalities (*46*).

Some genes had far more EPL connectivity than others, over a 10-fold range (Fig. 1C and data file S2). Such a spread was observed in nonimmunologic lineages, where some authors proposed to distinguish a class of "Super Interactive Promoters" (*47*, *48*). Here, such superconnected genes (523 in T_{reg} and 520 in T_{conv}) include several T_{reg} and T_{conv} hallmarks such as *Entpd1*, *Lef1*, *Ccr7*, *Cd5*, or *Lrrc32*. These superinteractive genes tend to be associated with "Super Enhancer" elements: Of the 65 superenhancers nominated in T_{regs} (*41*), 13 included superinteractive promoters (chisq $P < 0.01$).

Differences between T_{reg} and T_{conv} were readily identified, as exemplified by several prototypical T_{reg} signature transcripts. Several EPLs were observed at the *Ikzf2* promoter in T_{regs} but none significantly above background in T_{conv} (Fig. 1D). ATAC-seq accessibility patterns were essentially identical in T_{reg} and T_{conv} at these positions, however, suggesting that the locus is poised but not connected in T_{conv} (which do express *Ikzf2* upon activation). Reciprocal T_{reg} or T_{conv} patterns were observed for T_{reg} signature genes *Il2rb* and *Pde3b* (fig. S1E). Genome wide, we identified 10,168 (9% of total EPLs) differentially active EPLs [at fold change (FC) of >2, $P < 0.05$; Fig. 1E and fig. S2A]. Signal intensities in HiChIP data integrate true loop frequency and stability ("3D signal") with the total abundance of the mark targeted by the immunoprecipitation ("1D signal"; fig. S2, C to E) (*9*). Total EPL signal in HiChIP data could thus appear to change, even if there was no actual increase in loop abundance per se. Analysis of the variation of total (1D) H3K27Ac signal showed that the T_{reg}/T_{conv} differences in EPL intensity did represent increased looping, as they could not be accounted for by simple variation in H3K27Ac deposition, which varied very modestly (Fig. 1F). This degree of EPL variation between $CD4^+$ T subsets is generally more extensive than the disparity observed by chromatin accessibility (less than 1% difference in accessibility) (*32*). Some genes that prototypically distinguish T_{reg} and T_{conv} show differential EPLs (*Ikzf2*, *Lef1*, *Satb1*, *Il2ra*, and *Foxp3*; fig. S2B), consistent with observations in human T cells (*9*). Accordingly, pairing of gene expression and cumulative EPL intensity revealed a positive relationship between differential EPL intensity and mRNA levels between the two cell types (Fig. 1G).

FoxP3 preferentially targets hyperactive EPLs

Having established the overall landscape of EPLs in T_{reg} and T_{conv} cells, we performed HiChIP with anti-FoxP3 antibody to identify enhancer-promoter interactions that involve FoxP3, for clues to understand how it performs its central role in shaping T_{reg} identity. Data were generated in well-correlated biological duplicates (fig. S3A), with correction for proximity ligation and an irrelevant immunoglobulin G (IgG) control to ensure specificity (fig. S3, B and C). To help identify the most reliable FoxP3 EPLs, we leveraged existing FoxP3 ChIP-seq data (*32*, *41*) (fig. S3D) and filtered putative FoxP3 EPLs against this input (fig. S3E). We thus identified 13,681 robust FoxP3-decorated EPLs of ~20-kb median length (fig. S3F and Fig. 2A). FoxP3 EPLs connected enhancers to the promoters of an unexpectedly large number of genes (4797), confirming that FoxP3 relates to far more loci than just the ~500 genes of the T_{reg} signature. Here again, a subset of genes showed superconnectivity (Fig. 2B), enriched for T cell–specific ontologies (T activation $P = 10^{-12}$, cytokine signaling $P = 10^{-11}$) and T_{reg} signature genes (*Il2ra*, *Ikzf2*,

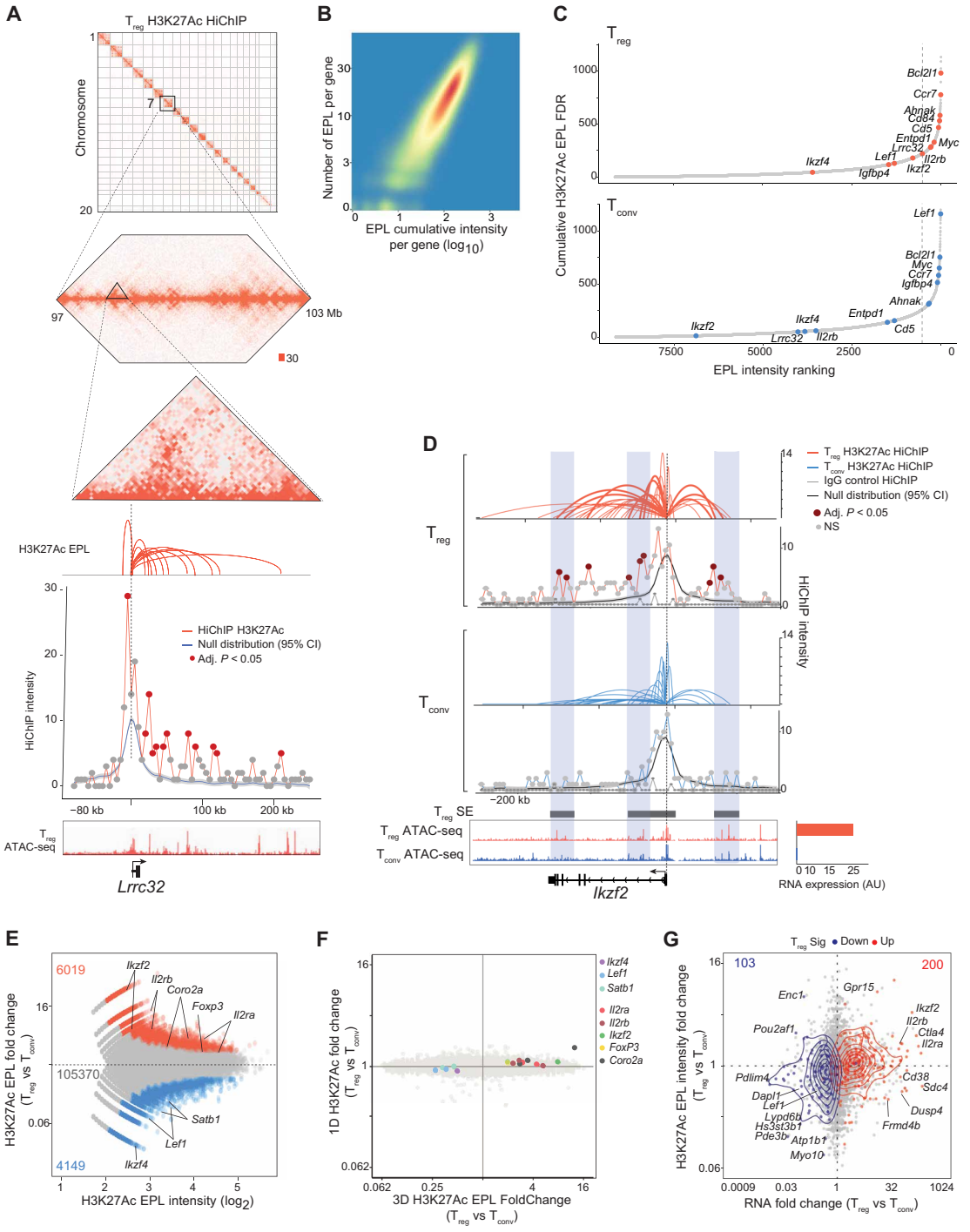

Fig. 1. T cell–specific EPLs sync with the transcriptional regulation of the T_{reg} gene program. (**A**) Profiling the genome-wide enhancer-promoter architectures of mouse regulatory T cells in vivo with H3K27Ac HiChIP. A focused view of the *Lrrc32* locus shows a null distribution based on random proximity-biased ligations [95% confidence interval (CI)] and those called as significant H3K27Ac HiChIP EPLs (FDR, 5%) in T_{regs}. (**B**) Scatter density plot of T_{reg} H3K27Ac HiChIP EPLs and the relative cumulative intensities (Pearson $r = 0.78$, $\log_{10}$). (**C**) Ranking plots of superinteractive promoters determined for H3K27Ac T_{reg} (top, $n = 523$ genes) and T_{conv} (bottom, $n = 520$ genes) using the summed cumulative H3K27Ac EPL FDRs, respectively. (**D**) T cell–specific enhancer-promoter configurations of the *Ikzf2* locus in T_{reg} (top) and T_{conv} (bottom) cells. Differential EPLs are considered as >2 FC and adjusted $P < 0.05$. IgG control HiChIP and null distributions (95% CI) are also shown for T_{regs} and T_{conv} cells. ATAC-seq genomic tracks and RNA expression for *Ikzf2* are shown for T_{regs} and T_{conv} cells, respectively. NS, not significant; AU, arbitrary units. (**E**) FC versus mean intensity (MA) plot of differential H3K27Ac HiChIP EPLs between T_{reg} (red) and T_{conv} (blue) cell types. EPLs with differential intensity (adjusted $P < 0.05$, FC > 2) are highlighted with numbers shown. (**F**) Comparison of 3D H3K27Ac HiChIP EPL intensities (*x* axis, FC in T_{reg} versus T_{conv}) and 1D H3K27Ac HiChIP EPL intensities (*y* axis, FC in T_{reg} versus T_{conv}). (**G**) Comparison of RNA expression (*x* axis, FC in T_{reg} versus T_{conv}) and cumulative H3K27Ac EPL intensities (*y* axis, FC in T_{reg} versus T_{conv}). Genes are colored as up (red) or down (blue) T_{reg} signature membership.

and *Entpd1*). As illustrated for *Entpd1* and *Il2ra*, prototypical T_{reg}-up signature genes, abundant FoxP3-decorated EPLs corresponded to FoxP3-binding enhancers identified by ChIP-seq (Fig. 2A and fig. S4A) and overlapped with a subset of the H3K27Ac EPLs. At both the *Lef1* and *Tcf7* loci, which are underexpressed in T_{regs}, FoxP3 EPLs also aligned with the positions of H3K27Ac EPLs, the latter being far less intense in T_{reg} than in T_{conv} cells, consistent with an inhibitory impact of FoxP3 (Fig. 2C and fig. S4C). At the *Il2* locus, two H3K27Ac EPLs were observed in T_{conv} (fig. S4B), but no loops whatsoever were detected in T_{reg}, whether in association with H3K27Ac or with FoxP3, suggesting that the locus is closed into heterochromatin independently of FoxP3.

We then analyzed the distribution of FoxP3 EPLs, beyond these examples, in gene sets that reflect differential expression in T_{regs} and

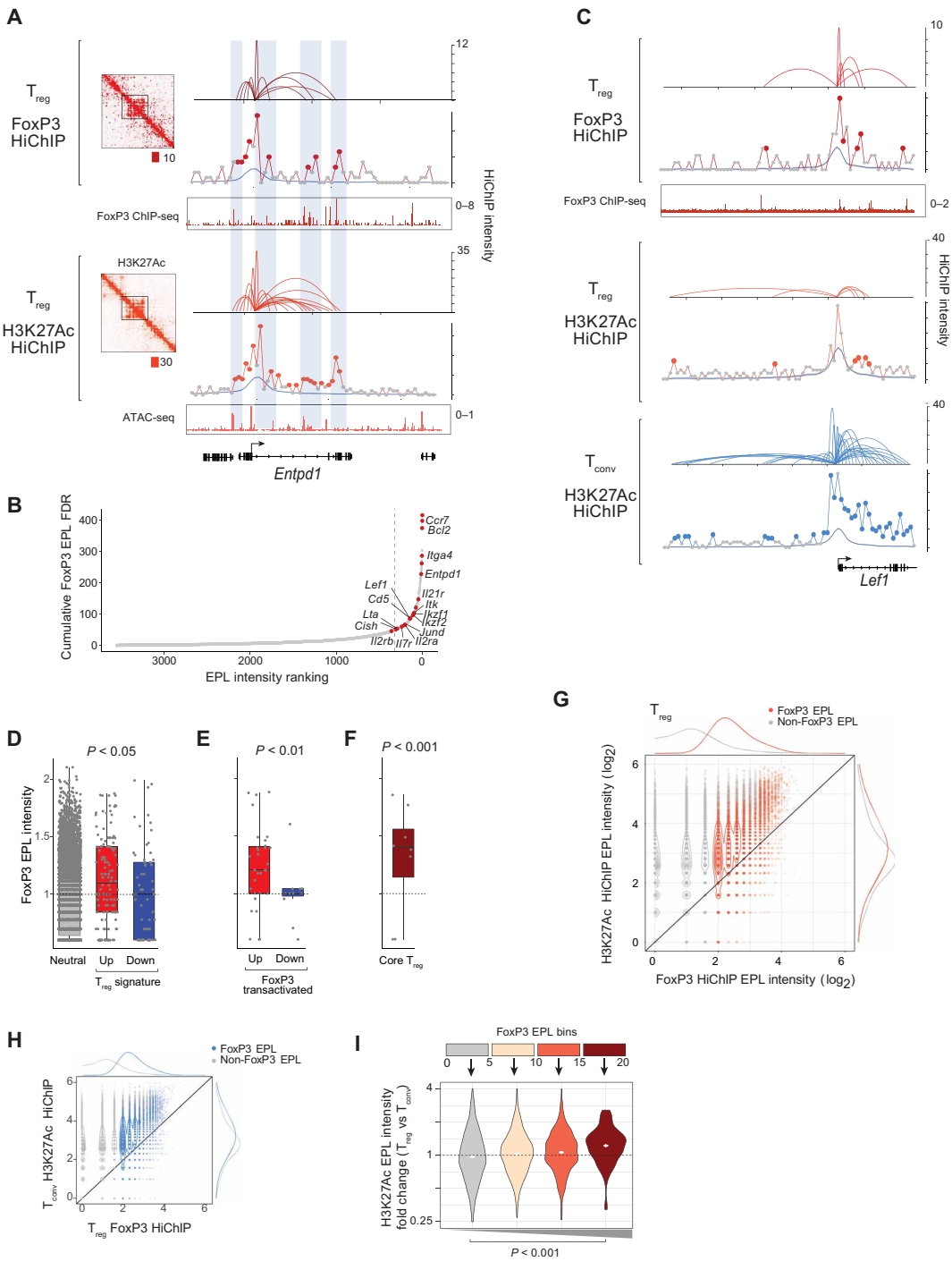

Fig. 2. Genome-wide T_{reg} FoxP3 enhancer-promoter looping generally associates with H3K27Ac-marked architectures. (**A**) T_{reg} FoxP3 (top) and T_{reg} H3K27Ac (bottom) EPLs shown for the target gene *Entpd1*. Highlighted areas emphasize the agreement between FoxP3 and H3K27Ac EPLs. (**B**) Rank plot of the FoxP3-specific superinteractive promoters ($n = 320$ genes). (**C**) FoxP3 (top), T_{reg} H3K27Ac (middle), and T_{conv} H3K27Ac (bottom) EPLs for the *Lef1* locus. (**D** to **F**) Boxplots of FoxP3 cumulative EPL intensities for the T_{reg} (D), FoxP3 transactivated (E), and core signatures (F). Significance was determined for T_{reg} up ($P < 0.05$), FoxP3 transactivated up ($P < 0.001$), and core T_{reg} ($P < 0.01$) gene sets using a *t* test. (**G**) Scatterplot of FoxP3 HiChIP EPL intensities (*x* axis, $\log_2$) and T_{reg} H3K27Ac HiChIP EPL intensities (*y* axis, $\log_2$). FoxP3-specific EPLs are highlighted. (**H**) Scatterplot of FoxP3 HiChIP EPL intensities (*x* axis, $\log_2$) and T_{conv} H3K27Ac HiChIP EPL intensities (*y* axis, $\log_2$). FoxP3-specific EPLs are highlighted. (**I**) FC distributions comparing H3K27Ac HiChIP EPL intensities (*y* axis, T_{reg} versus T_{conv}) for each FoxP3 EPL bin (*x* axis). Significance was determined using a *t* test ($P < 0.001$).

FoxP3 dependence. Classic "T_{reg} signature genes," which are known to have FoxP3-dependent and FoxP3-independent components (*39*, *49*), showed a modest but significant increase in cumulative FoxP3 EPL intensity compared with expression-matched "neutral" genes (Fig. 2D). This enrichment was accentuated in a set of FoxP3-dependent genes that are up-regulated after short-term FoxP3 transfection (Fig. 2E) (*31*). No such enrichment was seen for down-regulated targets (Fig. 2, D and E). The strongest enrichment in FoxP3-associated EPLs was seen for genes that constitute a core signature of FoxP3-dependent genes identified in FOXP3-deficient mice and patients (Fig. 2F) (*25*). These results are consistent with the notion that transcriptional up-regulation by FoxP3 is directly achieved through enhancer-promoter connections at up-regulated loci.

Overall, plotting the relationship between FoxP3 and H3K27Ac EPLs showed that FoxP3 EPLs correspond to loops with the highest level of H3K27Ac-associated signals (Fig. 2G), suggesting that FoxP3 associates with the most active chromatin. To ensure that this observation was not an experimental artifact, we performed HiChIP for the Yy1 TF, which is considered a structural regulator broadly involved in enhancer-promoter topologies (*17*, *50*). In T_{regs}, Yy1 represses *Foxp3* (*51*) and inhibits transactivation by FoxP3 protein (*31*, *51*). The 12,426 Yy1 EPLs thus identified were also

enriched in H3K27Ac HiChIP intensity when compared with non-Yy1 chromatin interactions ($P < 0.05$), similar to FoxP3 and consistent with observations in stem cells (*17*). However, FoxP3 and Yy1 EPLs showed differential EPL patterns (fig. S6, A and B), most notably at *Il2* (fig. S4B). In a combined set of FoxP3/or/Yy1 EPLs ($n = 21{,}341$), 54.3% were differentially represented (>2-fold difference in intensity). The genes associated with FoxP3 or Yy1 EPLs belonged to different functional classes: Yy1 EPLs were enriched in "general transcription" or "cell protein catabolism" ontologies, whereas FoxP3-associated EPLs belonged to more immune-specific pathways ("adaptive immune system" and "MHC-I presentation"; fig. S6C).

Examination in T_{conv} of those H3K27Ac EPLs that bind FoxP3 in T_{regs} revealed that most of them also had high intensity in T_{conv} (Fig. 2H). Thus, FoxP3 binds to EPLs that are very active in $CD4^+$ T cells in general and not solely to T_{reg}-specific ones, consistent with the notion that it homes to chromatin locales that are ubiquitously open in T cells (*32*, *33*). If FoxP3 locates to T_{reg} EPLs with the highest degree of activation, how does its presence affect them? To address this question, we compared the H3K27Ac EPL intensities of the EPLs in T_{regs}, where FoxP3 is bound, versus in T_{conv}, where FoxP3 is absent, across bins of FoxP3 EPL intensity. Increasing FoxP3 corresponded to increased H3K27Ac EPL signal at those EPLs in T_{regs} relative to T_{convs} (Fig. 2I), suggesting that FoxP3 may exert a facilitating influence on EPLs.

Direct tuning of FoxP3-dependent transcriptional programs through FoxP3 EPLs

Our results are compatible with, but do not prove, the notion that transcriptional activation by FoxP3 is actuated directly through enhancer-promoter connections around its target genes. However, this notion is at odds with the recent claim that FoxP3 shapes T_{reg} identity indirectly, by regulating the abundance of intermediary TFs like T cell factor 1 (TCF1) (encoded by *Tcf7*) (*52*). While we did observe FoxP3-decorated EPLs across the *Tcf7* locus (fig. S4C), the sweeping conclusion that indirect regulation shapes T_{reg} transcriptional identity is likely an overstatement, as discussed in detail elsewhere [see note in (*53*)]. Some indirect control probably occurs (because FoxP3 controls several other TFs), but a sizeable portion of the FoxP3-dependent transcriptome is likely to be directly controlled by FoxP3, including key functional transcripts. It was important, however, to verify that the FoxP3-decorated EPL structures reported here are functionally relevant. To this end, we performed H3K27Ac HiChIP on T_{reg}-like cells sorted from a novel FoxP3-deficient line [hereafter knockout–green fluorescent protein (KO-GFP; fig. S5, A to C), constructed from the classic FoxP3-IRES-GFP reporter mouse (*54*) by a CRISPR-engineered frameshift mutation that eliminates the Forkhead domain, resulting in a full *scurfy*-like T_{reg} deficiency phenotype; see Methods]. As other FoxP3-deficient mice [see (*25*) for references], KO-GFP mice contain a sizeable proportion of FoxP3-null T_{reg}-like cells (fig. S5, D and E), identifiable by activity of the GFP reporter appended to the disarmed *Foxp3* locus. Heterozygous females with one copy of this locus are protected from disease by the wild-type (WT) *Foxp3* allele (provided by a *Foxp3-Thy1.1* reporter chromosome to facilitate identification; fig. S5E). Genomic comparison to cells in which the intact Foxp3-GFP allele (hereafter WT-GFP) is active enables very precise determination of the effect of the FoxP3 deficiency in T_{reg}-like cells, identified by the same reporter configuration. We sorted WT-GFP and KO-GFP T_{regs} from half-sib heterozygous females (Fig. 3A) and performed H3K27Ac HiChIP to evaluate FoxP3's effects on enhancer-promoter looping.

Lieberman-Aiden *et al.* (*55*) showed that HiC and HiChIP data, when analyzed by principal components analysis, reveal spatial segregation of open and closed chromatin that forms two genome-wide compartments. By this measure, FoxP3 deficiency did not affect nuclear compartments on the macroscale, with no change in heterochromatin compartments identified by principal components analysis (Fig. 3, B and C). However, loci with rich FoxP3 EPLs, like *Ikzf2* and *Lrrc32*, showed significantly reduced H3K27Ac-decorated loops in FoxP3 KO T_{regs} (arrows in Fig. 3D, $P < 0.05$); these differences were reproducible in biological replicates (fig. S5F). As above, this reduction in EPL intensity in KO-GFP T_{regs} denoted a true loss of connectivity, not merely lower H3K27Ac decoration (Fig. 3E): The drop in H3K27Ac EPL intensity (x axis) was not accompanied by a drop in total "1D" H3K27Ac signal at these loci. Conversely, FoxP3 down-regulated targets *Lef1* and *Add3* showed increased H3K27Ac EPL signal in KO-GFP T_{regs} (fig. S5G). Comparing genome-wide H3K27Ac EPL abundance in WT-GFP and KO-GFP T_{reg}-like cells showed a general concordance, with only a light bulge for the most highly represented EPLs (Fig. 3F). This deviation was confirmed by plotting the KO-GFP/WT-GFP ratio of H3K27Ac EPL intensity across FoxP3 EPL intensity bins (Fig. 3G, $P < 0.01$), showing a clear reduction in signal resulting from the lack of FoxP3 in those EPLs with highest FoxP3 EPL intensity. The conclusion that FoxP3 directly shapes chromatin connectivity and its transcriptional relevance was confirmed by the cumulative density plot of KO/WT ratios for FoxP3 target genes defined as above (from direct transactivation studies or the core T_{reg} set; Fig. 3H). EPLs in FoxP3–up-regulated genes were more sensitive than the norm to the absence of FoxP3 (and the converse was true of FoxP3-repressed loci). These results support FoxP3's association to epigenetically active loops, through which it directly influences the T_{reg}-specific gene program.

Two different categories of FoxP3-dependent genes

These results show that, as a group, transcripts whose expression is up-regulated by FoxP3 are enriched in FoxP3-adorned EPLs, but this characteristic does not necessarily apply to all such genes. To further discriminate between loci with FoxP3-enhanced expression in T_{regs}, we compared accessibility in single cells: Similarly regulated genes tend to have correlated activity across individual cells, and correlation analysis can uncover groups of genes with similar regulatory logic (*56*, *57*). We used single-cell ATAC-seq (scATAC-seq) because chromatin accessibility is more stable than mRNA levels (*57*–*59*), generating high-quality scATAC-seq profiles for 5810 splenic T_{regs}, including resting T_{reg} (rT_{reg}) and activated T_{reg} (aT_{reg}) subsets (Fig. 4A). We first defined a FoxP3-dependent gene set from the expression data of van der Veeken *et al.* (*52*), by contrasting T_{reg}-like cells from heterozygous female mice in which FoxP3-deficient or FoxP3-proficient X chromosomes were active (fig. S6D; 377 up-regulated genes in FoxP3 proficient versus deficient at FC > 2 and $P < 0.01$). We generated a gene accessibility score from the scATAC-seq data and correlated these scores across all T_{regs} in the scATAC dataset. This gene-gene correlation network resolved into two predominant gene clusters (Fig. 4A), which exhibited a marked imbalance in FoxP3 EPL density (Fig. 4, B and C; $P < 0.01$, data file S3). Loci in cluster 1 had high FoxP3 EPL density (Fig. 4, B to D) and included many key T_{reg} transcripts (*Il2ra*, *Il2rb*, *Lrrc32*,

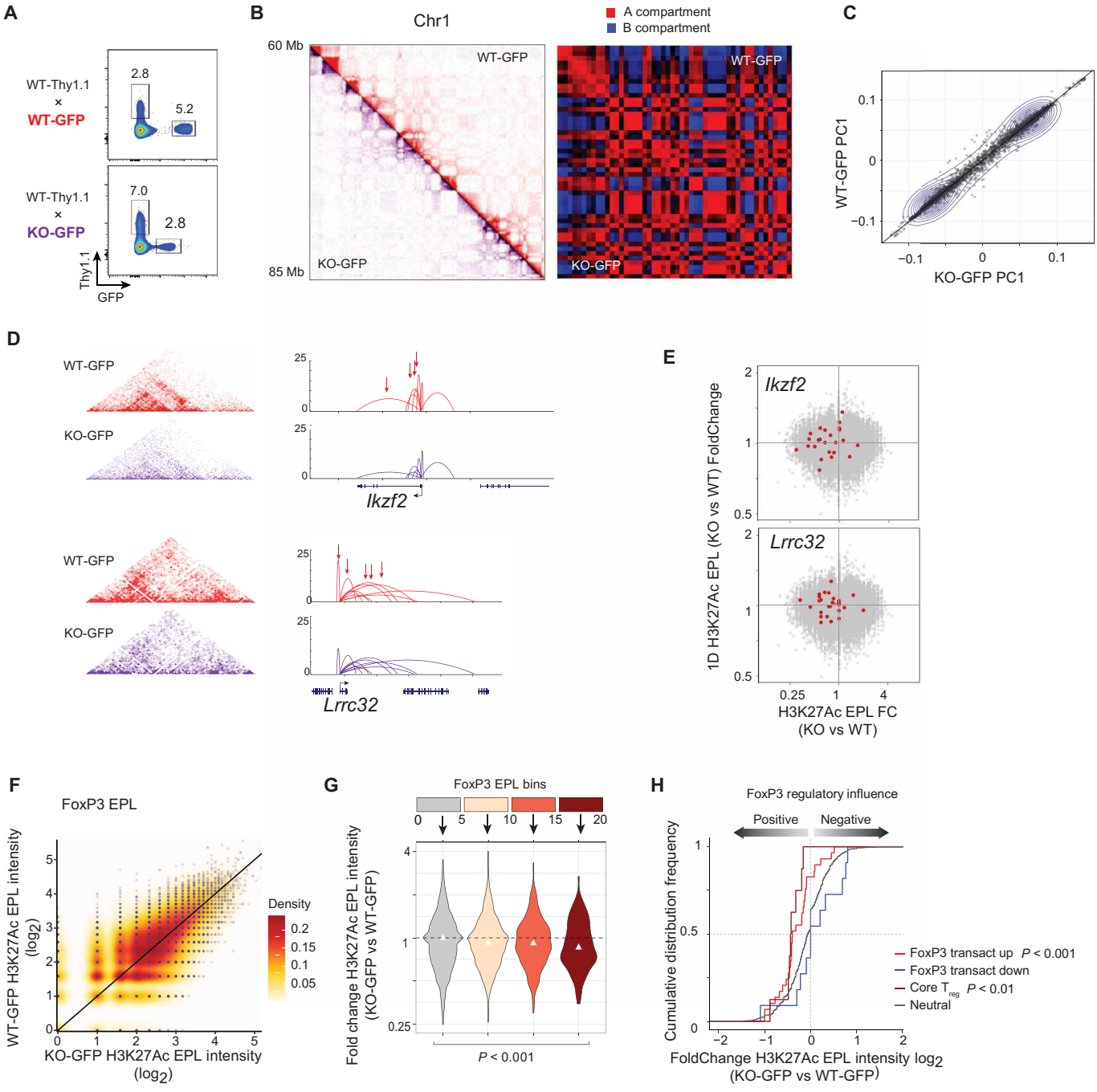

Fig. 3. FoxP3 enhancer-promoter looping directly modulates FoxP3-dependent transcriptional program. (**A**) FACS plots for WT-GFP–sorted (top) and KO-GFP–sorted (bottom) T_{reg} populations (gated on the $CD4^+TCR\beta^+$ population). (**B**) WT-GFP and KO-GFP intensity and chromatin compartment H3K27Ac HiChIP maps. (**C**) Genome-wide scatterplot of H3K27Ac HiChIP genome compartment scores (Pearson, 0.98). (**D**) WT-GFP (red) and KO-GFP (purple) H3K27Ac HiChIP intensity maps (left) and EPLs (right) of FoxP3 targets *Ikzf2* and *Lrrc32*. Arrows indicate EPLs FC > 1.5 and $P < 0.05$). (**E**) Comparison of 3D H3K27Ac HiChIP EPL intensities (*x* axis, FC in KO-GFP versus WT-GFP) and 1D H3K27Ac HiChIP intensities (*y* axis, FC in KO-GFP versus WT-GFP). *Ikzf2*- and *Lrrc32*-specific H3K27Ac EPLs are indicated. (**F**) Scatterplot of WT-GFP and KO-GFP H3K27Ac HiChIP EPL intensities for FoxP3-specific EPLs. (**G**) FC distributions comparing H3K27Ac HiChIP EPL intensities (*y* axis, KO-GFP versus WT-GFP) for each FoxP3 EPL bin (*x* axis). Significance was determined using a *t* test ($P < 0.01$). (**H**) Cumulative distribution frequency plot comparing KO-GFP and WT-GFP H3K27Ac EPL intensities for FoxP3 transactivated (up, $P < 0.001$) and core T_{reg} ($P < 0.01$) signatures. Significance was determined using a two-sample K-S test.

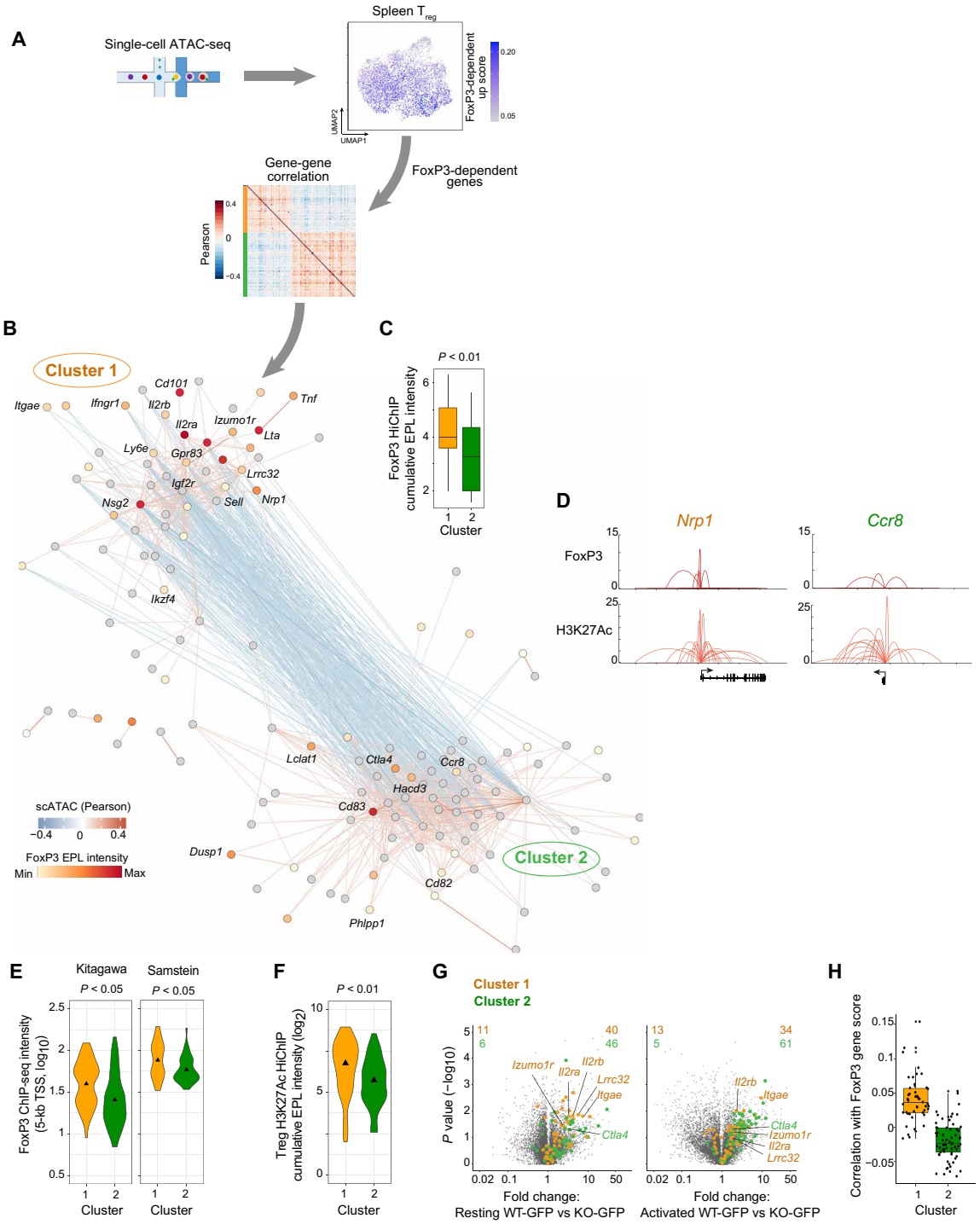

Fig. 4. Parsing the FoxP3-dependent coregulated network with single-cell chromatin accessibility. (**A**) Schema of splenic T_{reg} profiling with scATAC-seq. UMAP of splenic T_{regs} representing the FoxP3-dependent "up" signature gene score and gene-gene correlation heatmap (Pearson). (**B**) Gene scores were calculated from T_{reg} scATAC-seq for the FoxP3-dependent signature and represented as a force-directed network. Gene-gene correlations (edges) and FoxP3 EPL cumulative intensities for each gene (node) in the network are reflected by colored spectra. Indicated clusters were determined using both edge and node attributes. (**C**) Box plot comparing FoxP3 HiChIP cumulative EPL intensities for cluster 1 (orange) and cluster 2 (green) genes. Significance was determined between groups using a *t* test ($P < 0.01$). (**D**) FoxP3 and H3K27Ac HiChIP EPLs are shown for cluster 1 gene *Nrp1* and cluster 2 gene *Ccr8*. (**E**) Violin plots of FoxP3 ChIP-seq intensities between cluster 1 and cluster 2 gene sets. ChIP-seq signal was measured in a 5-kb window around the TSS. Significance was determined between groups using a *t* test ($P < 0.05$). (**F**) Violin plots of T_{reg} H3K27Ac cumulative EPL intensities between cluster 1 and cluster 2 gene sets. Significance was determined between groups using a *t* test ($P < 0.01$). (**G**) Volcano plots comparing the transcript expression of resting and aT_{regs} (WT-GFP versus KO-GFP). Gene clusters from (B) are highlighted. (**H**) scATAC gene activity score correlations (Pearson) between FoxP3 and individual genes from cluster 1 and cluster 2 identified in (B).

Izumo1r, and *Nrp1*), predominantly characteristic of rT_{regs}; in contrast, genes of cluster 2 showed much lower FoxP3 EPL density and corresponded mainly to transcripts enriched in aT_{regs} (e.g., *Ccr8*; Fig. 4D). Accordingly, genes from cluster 1 showed higher binding to FoxP3 in published ChIP-seq datasets (Fig. 4E), with H3K27Ac EPL intensity also biased for cluster 1 transcripts (Fig. 4F). Overall, cluster 1 genes tended to be expressed at somewhat higher levels than cluster 2 [median of 341 transcripts per million (tpm), 0.05 to 0.95 range (27 to 3576) versus 76 (26 to 1417)], but genes in both clusters were up-regulated by FoxP3 and overexpressed in WT relative to FoxP3-deficient T_{reg}-like cells (Fig. 4G).

We then asked, across all single cells, how the expression of individual genes of clusters 1 and 2 (approximated by the "gene accessibility score") correlated with that of FoxP3. The rationale was that, whereas all these genes appear FoxP3 dependent (as defined by the "sledgehammer" effect of FoxP3 deletion), their instant expression may respond differently to fluctuations in FoxP3 between individual cells. Cluster 1 genes had some positive correlation with Foxp3 (Fig. 4H). In contrast, genes of cluster 2, which are largely devoid of FoxP3-decorated EPLs, lacked this correlation (and was even slightly negative on average). This dichotomy might actually be what one would expect if cluster 1 were under direct and positive activation by FoxP3, whereas cluster 2 genes responded to indirect control by FoxP3. Thus, the partition of FoxP3-dependent genes into clusters independently marked by FoxP3 EPL density suggests that different regulatory mechanisms are at play in the different groups of FoxP3-dependent genes, with different levels of direct FoxP3 involvement.

Distinct FoxP3 interaction at promoters and enhancers

FoxP3 binding across the T_{reg} genome occurs at distal enhancers and in proximal promoter regions (*32*, *41*). It is unknown whether FoxP3 functions similarly in both locations. We assessed whether FoxP3 bound to the promoter or enhancer ends of the loops, based on the consensus ChIP-seq map described above. EPLs associated with FoxP3 on either promoter or enhancer sides or both (Fig. 5A). This dichotomy was unrelated to the clusters of Fig. 4 and not merely due to sparse sampling or arbitrary thresholds because FoxP3 binding was truly absent on the "other" side (Fig. 5B). Further, EPLs with FoxP3 on both sides were not a random occurrence because they occurred more frequently than through chance association (chisq $P < 0.01$). High chromatin accessibility and H3K27Ac signal intensity coincided with the side of the EPL bound by FoxP3 (fig. S7A), confirming FoxP3's association with the most highly active chromatin. A clue as to the significance of FoxP3 placement relative to EPL ends came from Gene Ontology analysis of the corresponding genes. Generic programs linked to nucleic acid metabolism (e.g., cell cycle and DNA repair) dominated for genes with promoter-side FoxP3 EPL, whereas more immune-specific ontologies (cytokine signaling and adaptive immune system) were enriched among enhancer- and dual-sided modes (Fig. 5C and data file S4). FoxP3-dependent loci belonging to cluster 1 described above were predominantly associated with enhancers (only 3 of 24 were of the promoter-side category).

FoxP3 collaborates with other TFs; these interactions determining its transcriptional specificity (*26*, *27*, *31*) and their binding motifs are enriched in the vicinity of FoxP3-binding sites (*32*, *41*). FoxP3 positioned at either the promoter or enhancer sides of EPLs appears to interact with distinct cofactors (Fig. 5D and fig. S7B), as shown by motif enrichment analysis (using as background comparators all TSS and all non-TSS OCRs, respectively). TATA-box motifs were enriched at promoter positions, whereas Runx and Ctcf motifs were overrepresented at enhancers, and motifs for SP1, Ets, Irf/Stat, and the nuclear receptor family factors (Rorα/γ) were enriched on both sides. Together, these results delineate different aspects of FoxP3-mediated regulation, with distinctive transcription programs and TF cofactor preference across FoxP3 EPLs.

DISCUSSION

To better understand the program controlled by the lineage-identifying factor FoxP3, we explored enhancer-promoter connectivity in true T_{reg} and T_{conv} cells ex vivo and how FoxP3 is associated with this architecture. The results lay out the landscape of enhancer elements that are connected to promoters of different genes in $CD4^+$ T cells and should thus serve as a roadmap to support cis-regulation studies in these cells. Reinforcing the identity of FoxP3 as a positive transactivator, they establish how FoxP3 associates with a wide range of active EPLs and positively potentiates their representation for a set of genes that are central to T_{reg} physiology.

Previous models of enhancer regulation (*46*, *60*–*62*) have hypothesized additive or even multiplicative enhancer activity. In the primary cells analyzed here, there was a significant but modest correlation between enhancer-promoter connectivity and mRNA levels in these two closely related $CD4^+$ T cells. The absence of a linear relationship is consistent with the notion that simply establishing a connection between an enhancer and a promoter is not sufficient for transactivation but that secondary events (recruitment of additional factors and posttranslational modification of these cofactors) are necessary to functionally potentiate the connection. Cumulative EPL intensities for individual genes distributed as a very broad range, with a subset of highly connected T cell genes, in line with recent work in neurons which identified a subset of "superinteractive promoters" (*48*). Such highly connected loci may be rationalized by the need for more complex transcriptional hubs for variegated regulation.

A key goal was to understand whether and how FoxP3 is involved with enhancer-promoter connectivity. Does it promote loop formation or tune the transactivation potential of preestablished loops—the latter in keeping with the observation that, unlike other TFs that specify immunocyte lineages such as PU.1 or Pax5, FoxP3 opportunistically exploits already open chromatin and has limited "pioneer" activity—or does it have little influence, only acting indirectly, as suggested elsewhere (*52*)? In general, FoxP3 associated with the most epigenetically active chromatin, as did Yy1. Several lines of evidence established that, once associated with an EPL, FoxP3 mostly exerts an enhancing influence on enhancer-promoter connectivity, e.g., by stabilizing them: (i) H3K27Ac EPLs that are also associated with FoxP3 in T_{regs} are more intense in T_{regs} than they are in T_{convs}; (ii) these same EPLs lose intensity when FoxP3 is genetically inactivated; in other words, when FoxP3 is absent, these enhancers are less connected to their cognate promoters. The functional relevance of these effects is established by the observation that these enhanced connections are found for genes whose expression is known to be positively transactivated by FoxP3.

Different generations of chromatin immunoprecipitation (*31*, *32*, *41*, *52*, *63*, *64*) showed that FoxP3 associates with many genomic regions that are nowhere near the T_{reg}-specific loci. In this, FoxP3 is not unlike many other TFs (*65*). Our results now show that

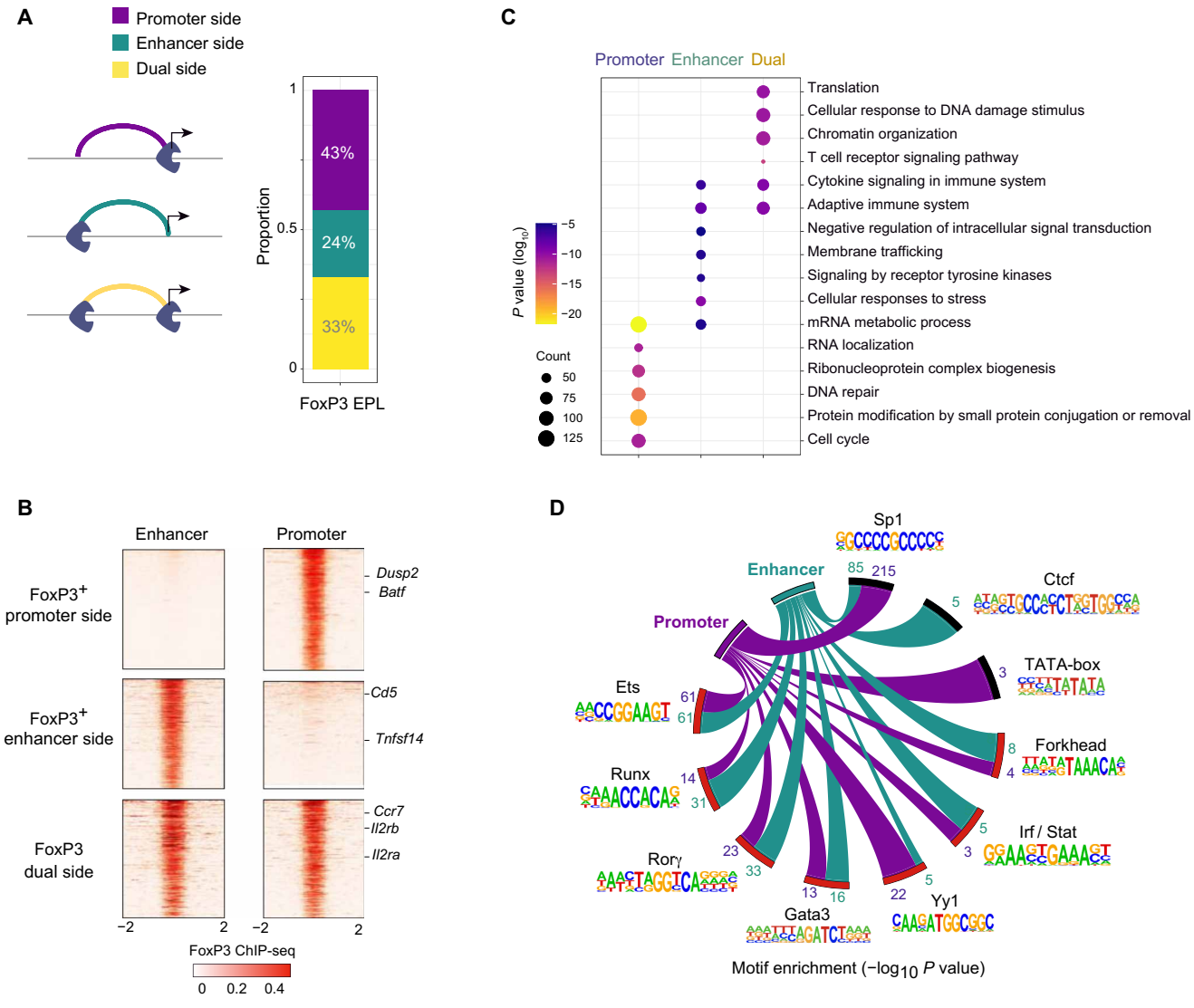

Fig. 5. FoxP3 positioning at EPLs distinguishes gene and TF-motif components. (**A**) FoxP3 HiChIP EPL proportions based on FoxP3-binding modes fixed on either the promoter, enhancer, or dual sides of FoxP3 loops. (**B**) FoxP3 ChIP-seq heatmaps centered on FoxP3 bound position within EPLs for promoter, enhancer, and dual modes. (**C**) Gene Ontology enrichments based on FoxP3 HiChIP EPL mode. Size of circle indicates number of genes, and color represents significance (*P* value). (**D**) Circos plot of TF motif enrichments for promoter and enhancer FoxP3 HiChIP EPLs. Arc thickness defines TF motif significance ($-\log_{10} P$ value).

these apparently inactive locations actually correspond to true enhancer-promoter connections, even at loci that have no clear T_{reg} relevance (38% of T_{reg}-neutral genes have a FoxP3-decorated EPL). An interpretation consistent with the cofactor model is that these positions simply lack the appropriate cofactors or epigenetic modifying enzymes or that FoxP3 or its cofactors are not suitably modified at these locations to actually influence transcription. FoxP3 may be truly inert at these locations, or it might provide buffering or stabilizing influence (*61*, *62*, *65*). At FoxP3-dependent loci that are overexpressed in T_{regs}, high-intensity FoxP3 EPLs were observed at many core signature genes, which strongly suggest a positive and direct transactivation, in contrast to the indirect model recently proposed (*52*). In contrast, an indirect modality for FoxP3-dependent repression is consistent with the dearth of FoxP3 EPLs at the *Il2* locus. But indirect repression by FoxP3 is not a general characteristic of T_{reg}-underexpressed loci because *Lef1* and *Tcf7* genes themselves show abundant FoxP3-associated EPLs, consistent with the notion that FoxP3 can act as a direct repressor when paired with the appropriate cofactors (*31*).

Last, the dichotomy between loci at which FoxP3 associates on the enhancer or the promoter sides of EPLs implies a geographical variation of its direct regulatory functions. This demarcation parallels recent results in B cells where distinct multi-TF hubs bind to promoter versus distal enhancer sites (*66*). The enrichment analysis (Fig. 5D) suggests that the factors with which FoxP3 associates on the enhancer or the promoter sides are different, suggesting different modes of operation. It is also possible that this repartition is dynamic [per (*12*, *13*)], and one could speculate for instance that, upon rapidly acting cell triggering, FoxP3 already bound to the promoter region serves to further stabilize/potentiate an EPL through dimerization with another FoxP3 molecule recruited to the enhancer side.

In terms of how FoxP3 determines T_{reg} identity, parsing the group of FoxP3-dependent genes by correlation analysis of chromatin accessibility across single T_{regs} distinguished two groups of genes, among those positively controlled by FoxP3. The larger cluster was associated with abundant FoxP3-decorated EPLs, indicative of direct and positive transactivation. The second, smaller, cluster grouped genes are associated with markedly less FoxP3-bound EPLs. Genes of this second cluster include genes that are overexpressed in aT_{reg} relative to rT_{reg}, and these might correspond to indirect control (*52*).

These results, as well as those from (*25*) and (*52*), suggest a multimodal set of actions through which FoxP3 helps determine T_{reg} identity and stability: (i) direct control, both activating and repressive, of a range of target loci, particularly a core set of transcripts essential for T_{reg} homeostasis; (ii) repression of TFs that otherwise favor the T_{conv} program; (iii) stabilization of a T_{reg} program that is not directly FoxP3 dependent.

MATERIALS AND METHODS

Study design

The control of T_{reg}-specific gene expression is mediated by the action of FoxP3 on chromatin. To derive the direct mode of FoxP3 activity on chromatin, we biochemically mapped FoxP3-associated EPLs using HiChIP in primary mouse T_{regs}. Mapping FoxP3 EPLs on a general roadmap of enhancer-promoter looping mediated by HiChIP H3K27Ac in T_{conv} and T_{regs} provided a deeper understanding of FoxP3-specific control on its target genes. Specificity of HiChIP experiments was ensured by including biological replicates, a negative isotype IgG control HiChIP, comparable sequencing depth across samples, and prioritizing EPLs using a null model of proximity ligation events. We validated the extent of FoxP3-associated EPLs in promoting active regulation of its targets through generation of a FoxP3 KO mouse model. H3K27Ac HiChIP of FoxP3-WT and FoxP3-KO T_{regs} shifted EPL activity at FoxP3-associated EPLs and core T_{reg} programs. To address the direct nature of FoxP3 on gene targets, we integrated T_{reg} scATAC-seq and FoxP3 EPLs, which resolved specific cluster of T_{reg}-specific transcripts that covary in their chromatin accessibility and are directly controlled by FoxP3 looping.

Mice

C57BL/6J (B6) and B6.*Foxp3*$^{Thy1.1}$ (*67*) mice were obtained from the Jackson Laboratory and bred in the specific pathogen–free facility at Harvard Medical School (HMS). All experimentation was performed following animal protocols approved by the HMS Institutional Animal Use and Care Committee (protocol IS00000054). FoxP3-deficient mice (B6.*Foxp3*$^{fs327\text{-}gfp/Doi}$) were generated by CRISPR mutagenesis of the B6.*Foxp3*$^{ires\text{-}GFPKuch}$ line (*54*). Briefly, the Foxp3-IRES-GFP allele carries a 1-bp insertion in exon 11 (NM_054039.2), at the position encoding FoxP3 amino acid 327, leading to a frameshift mutation that would produce a truncated protein terminating after 34 amino acids and thus lacking the essential C-terminal forkhead DNA binding domain (fig. S5A). Males carrying the mutant allele present with a typical *Scurfy*-like phenotype of FoxP3 deficiency, with a wasting syndrome starting at 12 to 15 days of age (failure to thrive, cachexia, extensive exfoliative dermatitis, tail necrosis, crusty eyelids and ears, marked lymphadenopathy, and splenomegaly) leading to death around 30 to 35 days. Heterozygous females are healthy and do not show any clinical signs of inflammation. The germline mutation was maintained onto the B6 background. For the experiments reported here, females carrying either the normal *Foxp3*$^{ires\text{-}GFPKuch}$ or the deficient *Foxp3*$^{fs327\text{-}gfp}$ alleles were crossed to B6.*Foxp3*$^{Thy1.1}$ father (the FoxP3-Thy1.1 reporter was used to identify in the offspring normal T_{regs} that express the WT balancing allele in these crosses). To improve the comparability between parallel fs327 and WT offspring in these experiments, the *Foxp3*$^{ires\text{-}GFPKuch}$ and *Foxp3*$^{fs327\text{-}gfp}$ carrier mothers were cohoused and bred to the same B6.*Foxp3*$^{Thy1.1}$ father.

T cell isolation

For analyses in FoxP3-proficient mice, splenic CD4$^+$ T cells from FoxP3-Thy1.1 hemizygous male mice were first enriched using a CD4 untouched kit (Miltenyi), followed by secondary purification with anti-CD90.1 microbeads (Miltenyi) according to manufacturer's instructions. T_{conv} (FoxP3$^-$Thy1.1$^-$Tcrb$^+$CD4$^+$CD45$^+$CD19$^-$CD8$^-$CD11b$^-$CD11c$^-$) and T_{reg}^s (FoxP3$^-$Thy1.1$^+$Tcrb$^+$CD4$^+$ and CD45$^+$CD19$^-$CD8$^-$CD11b$^-$CD11c$^-$) were sorted on a FACS-Aria to 96 and 94% purity, respectively. For experiments in FoxP3-deficient T_{regs} (Fig. 3), CD4$^+$ T cells from spleen and peripheral lymph nodes from 6-week-old heterozygous females were first enriched as above by negative magnetic selection (STEMCELL Technologies), and T_{reg}-like cells were sorted as CD19$^-$TCRβ$^+$CD4$^+$Thy1.1$^-$GFP$^+$ on a Moflo Astrios (Beckman Coulter).

H3K27Ac, FoxP3, Yy1, and IgG HiChIP

HiChIP (*9*) was optimized and performed in biological replicates for all conditions. Briefly, 5×10^6 T_{regs} were cross-linked for each FoxP3 HiChIP replicate, 2×10^6 million cells for H3K27Ac and Yy1 HiChIPs, respectively. In addition, 5×10^6 million T_{regs} and T_{conv} cells were cross-linked to include a negative IgG isotype control HiChIP samples. Low-input H3K27Ac HiChIP was performed on 2×10^5 cross-linked WT-GFP and KO-GFP T_{regs}, respectively. DNA sonication of fragments to 200 to 600 bp after Mbo I digestion was performed using the Covaris M220. Sonicated DNA was precleared using Protein A magnetic beads followed by overnight chromatin immunoprecipitations with 3 μg of H3K27Ac (Abcam ab4729), 5 μg of FoxP3 (Abcam ab150743), 3 μg of Yy1 (Abcam ab109237), and 5 μg of rabbit IgG (Cell Signaling Technology, 2729S), in a final concentration of 0.07% SDS. Libraries were prepared using an Illumina Nextera DNA library preparation kit, size-selected using low-melt gel extraction, and paired-end–sequenced using NextSeq 500 Illumina platform.

Single-cell ATAC-seq

scATAC-seq data were generated as part of another study. Briefly, splenic T_{regs} (CD4$^+$, TCRβ$^+$, and FoxP3$^-$IRES$^-$GFP$^+$) and T_{conv} cells (CD4$^+$, TCRβ$^+$, and FoxP3$^-$IRES$^-$GFP$^-$) were sorted from 6- to 8-week-old B6 FoxP3-IRES-GFP mice into Dulbecco's modified Eagle's medium + 2% fetal calf serum and then resuspended in phosphate-buffered saline + 0.04% bovine serum albumin. Nuclei isolation, transposition, Gel Bead-In EMulsions (GEM) generation, and library construction targeting capture of ~12,000 cells (75% T_{regs} and 25% T_{conv}) were carried out as detailed in the Chromium Next GEM Single Cell ATAC manual (10x Genomics). Libraries were pooled and sequenced on an Illumina NovaSeq to a final median depth of about 30,000 reads per cell (~80% saturation).

RNA-seq expression data

T_{reg} and T_{conv} RNA sequencing (RNA-seq) biological replicates were from previous work (*33*). RNA-seq counts were used for all gene quantification. Genes were filtered on the basis of replicated and cell

type expression; >10 counts in both replicates and in at least one condition.

ChIP-seq data

ChIP-seq datasets [Kitagawa *et al.* (*41*)]; Runx1, FoxP3, Ets1, Smc1a (Cohesin) [Samstein *et al.* (*32*)]; and FoxP3 were mapped to mm10 genome using bowtie2 (*68*). BigWig files were generated using deeptools2 (*69*).

ATAC-seq data

T_{reg} and T_{conv} ATAC-seq datasets were generated in previous work (*33*).

CAGE data

T_{reg} Cap Analysis of Gene Expression (CAGE) data were downloaded from the FANTOM repository (*70*).

scATAC-seq analysis

Fastq data were aligned to the mm10 reference genome and quantified per cell using Cell Ranger ATAC software (10x Genomics, v1.2). Peak by cell count matrices were generated by mapping reads to OCRs previously defined by the ImmGen consortium (*33*). Data analysis was performed using Signac v1.1 (*71*). For quality control, only cells with at least 4000 fragments per cell, greater than 55% reads in peaks, TSS enrichment score greater than 2, nucleosome signal less than 10, and ratio of blacklist-region reads less than 0.05 were retained for further analysis. Putative doublets identified by ArchR v0.9.3 (*72*) and non-T_{reg}, non-T_{conv} contaminant cells were also removed. We used the latent semantic indexing approach as previously described (*59*, *73*). Binarized count matrices were normalized using the term frequency–inverse document frequency transformation and reduced in dimensionality by singular value decomposition (SVD). Because the first SVD component was highly correlated with sequencing depth, components 2 to 30 were used to create a 2D uniform manifold approximation and projection (UMAP) visualization. A gene accessibility score was determined from T_{reg} scATAC-seq data with ArchR v0.9.3, using an exponentially weighted function that accounts for the activity of distal OCRs in a distance-dependent manner (*72*) and computes a single measure of a gene's accessibility. A gene-gene correlation was next determined from the log-normalized gene scores and visualized using a force-directed network (edge-weighted using correlation coefficients). The network was filtered to drop weak correlations (−0.2> and <0.2). Network clustering was performed using correlation coefficients (edge attribute) and FoxP3 EPL intensities (node attribute). Network visualization and clustering were performed using Cytoscape v3.8.0 (*74*).

H3K27Ac, FoxP3, and Yy1 HiChIP data processing and enhancer-promoter looping

HiChIP paired-end reads were aligned to the mm10 genome using the HiC-Pro pipeline (*75*). Default settings were used for removal of duplicated reads, assignment to Mbo I restriction fragments, and filtering for valid interactions. To assess EPLs in HiChIP data, we computed ±250-kb contacts from the gene TSS for 9058 expressed genes in T_{regs} and T_{conv} using the hicPlotViewpoint (*76*) function at a resolution of 5 kb. To assess a background proximity ligation frequency for each HiChIP experiment, we first generated a ligation probability background by sampling 1000 randomly selected intragenic regions more than 10 kb from the promoter and computing the relative counts using a window of ±250 kb in each HiChIP experiment. For each respective distance position, a Z-statistic was computed using the HiChIP background estimation, and adjusted *P* values were calculated to assess statistical significance of the contact. This procedure removed from 50 to 80% of noisy and biased chromatin interactions. Significant EPLs were considered if demonstrated enrichment across replicates, passing an FDR of 5% for H3K27Ac EPLs (n = 115,538) and 10% for Yy1 (12,426 EPLs), and enriched with respect to the negative control IgG HiChIP. In a similar manner, FoxP3 EPLs were also further analyzed using a reproducible set of overlapping 13,982 FoxP3 ChIP-seq peaks (*32*, *41*) as anchors. All FoxP3 EPLs (10% FDR) were supported by FoxP3 ChIP-seq binding for at least one end of the FoxP3 loop. 1D H3K27Ac HiChIP analysis was performed using all reads (including religation and dangling ends but excluding extrachromosomal contacts) and converted into tabular format [bedpe, using cLoops2 (*77*)] for downstream analysis. For each H3K27Ac EPL, 1D HiChIP signal was established for both the TSS and for distal anchor, and these were summed. Per-gene 1D H3K27Ac cumulative signal was calculated by summing 1D signal corresponding to all respective EPLs for each gene. Compartment analysis of WT-GFP and KO-GFP HiChIP was performed at 250-kb resolution using the eigenvector function on Knight-Ruiz (KR)-normalized maps (*78*).

Cumulative EPL intensities determined for genes

To measure the overall effect of the enhancer-promoter structure for a given gene, we calculated a single cumulative value by summing the respective HiChIP EPL intensities (H3K27Ac, FoxP3, and Yy1). In addition, the degree in connectivity was calculated by summing the total number of EPLs per gene and compared both with genome-wide expression and binned mRNA quantiles.

Superinteractive promoter analysis

To identify superinteractive promoters (SIPs) from T_{reg} and T_{conv} H3K27Ac or FoxP3 HiChIP, we followed a similar strategy used by (*48*, *79*). Briefly, for each gene, we summed the $\log_{10}$ FDR for respective EPLs to derive a single cumulative score per gene. Plots of the ranked cumulative interaction scores in each cell type and condition were plotted. Significant SIPs were determined on the basis of the point of inflection within the curve (slope is equal to 1).

Differential H3K27Ac EPL analysis

Differential H3K27Ac EPLs were identified using biological replicate EPL counts of T_{reg} and T_{conv} EPLs (P adjusted < 0.05, FC > 2) determined using diffloop (*80*). Cumulative H3K27Ac EPL differences and comparisons with gene expression between T cells were mapped for all genes and specifically highlighted for the up- and down-regulated T_{reg} signature program (*39*).

Yy1 and FoxP3 comparative analysis

Yy1 EPL and cumulative intensities were compared with FoxP3, respectively, to identify TF-specific interactions (twofold, $P < 0.05$). Gene Ontology analysis was performed for genes with differences between FoxP3 and Yy1 cumulative EPL intensities (twofold) using Metascape (*81*).

Deriving a FoxP3-dependent signature from RNA-seq data

Data from GSE154680 (*52*) were downloaded. Raw read counts tables were normalized by median of ratios method with DESeq2 (*82*) and converted to GCT and CLS formats. Genes with a minimum average read count of 35 in at least one group and a coefficient of

variation intrareplicate less than 0.30 to 0.45 were retained. An uncorrected *t* test was used to compute differential gene expression between the different groups from the normalized read counts dataset. The FoxP3-dependent gene signature list was computed by merging the differential expressed genes from the aT_{reg} and rT_{reg} datasets, comparing Foxp3-GFP-DTR WT versus Foxp3-GFP KO and an FC of >2 or <0.5 and a *P* value of <0.01.

Promoter, enhancer, and dual modes in FoxP3 looping

FoxP3 ChIP-seq binding data were used to parse FoxP3 EPLs into those with FoxP3 occupancy at promoter, enhancer, or both (dual mode) ends of EPLs. Genomic heatmaps (*69*) were generated for each group either centered on FoxP3-bound positions in FoxP3 EPLs or centered on the strongest T_{reg} ATAC-seq OCR for FoxP3-negative sides of the EPL. Gene Ontology analysis of FoxP3 modes were generated using Metascape (*81*). De novo motif analysis was performed using HOMER for FoxP3-bound positions of promoter and enhancer EPL modalities. Significant motifs were determined using as background comparisons using equal numbers (10,000) in TSS and non-TSS OCRs. Motif significance was represented for promoter and enhancer FoxP3 modes using Circos plots (*83*).

Il2 and *Il2ra* centric loop analysis

To resolve higher-resolution sets of chromatin loops, we first defined potential anchors from OCRs with accessibility in T_{conv} or T_{regs} (297,076 OCRs). HiChIP loops were defined from our OCR anchor set using Hichipper (*84*) (-peak-pad, 250 bp), which adopts a restriction fragment bias-aware approach for preprocessing of HiChIP data to call loops. Briefly, anchors were padded 250 bp in either direction and were considered if they overlapped MboI motifs. Padding anchors boost the number of paired-end tags that can be mapped to loops, respectively. We removed self-ligation loops and filtered loops that may be biased due to proximity (<3 kb) or low paired-end tag counts using the Mango (*85*) correction step (stage 5). This correction aggregates paired-end tag counts across all samples and retains significant loops (FDR < 0.01). A union set of loops across all data was generated: (i) loops with a minimum of two counts in both biological replicates, (ii) supported in at least one sample across all HiChIP experiments, and (iii) greater than twofold compared with IgG HiChIP controls. We mapped the hichipper-defined loops based on overlapping HiChIP EPLs for FoxP3, H3K27Ac, and Yy1 centering on the *Il2ra* and *Il2* locus.

Data visualization

Analysis was performed using R-3.5.2 with all plots generated using ggplot2 (https://ggplot2.tidyverse.org) (*86*). Statistical tests are described in their respective sections. Browser and genome views of ATAC-seq and ChIP-seq data were generated using UCSC (*87*) and IGV (*88*). EPL arc plots were generated using DNARchitect (*89*). HiChIP heatmaps were generated using HiC-Pro by merging valid pairs of replicates and processed as .hic files using the hicpro2juicebox function (*75*) and visualized using Juicebox tools (*78*).

SUPPLEMENTARY MATERIALS

www.science.org/doi/10.1126/sciimmunol.abj9836
Figs. S1 to S7
Table S1
Data files S1 to S4

View/request a protocol for this paper from *Bio-protocol*.

REFERENCES AND NOTES

1. R. Schleif, DNA looping. *Science* **240**, 127–128 (1988).
2. M. Ptashne, How eukaryotic transcriptional activators work. *Nature* **335**, 683–689 (1988).
3. M. Levine, C. Cattoglio, R. Tjian, Looping back to leap forward: Transcription enters a new era. *Cell* **157**, 13–25 (2014).
4. E. E. M. Furlong, M. Levine, Developmental enhancers and chromosome topology. *Science* **361**, 1341–1345 (2018).
5. S. Schoenfelder, P. Fraser, Long-range enhancer-promoter contacts in gene expression control. *Nat. Rev. Genet.* **20**, 437–455 (2019).
6. A. Field, K. Adelman, Evaluating enhancer function and transcription. *Annu. Rev. Biochem.* **89**, 213–234 (2020).
7. A. J. Rubin, B. C. Barajas, M. Furlan-Magaril, V. Lopez-Pajares, M. R. Mumbach, I. Howard, D. S. Kim, L. D. Boxer, J. Cairns, M. Spivakov, S. W. Wingett, M. Shi, Z. Zhao, W. J. Greenleaf, A. Kundaje, M. Snyder, H. Y. Chang, P. Fraser, P. A. Khavari, Lineage-specific dynamic and pre-established enhancer-promoter contacts cooperate in terminal differentiation. *Nat. Genet.* **49**, 1522–1528 (2017).
8. B. M. Javierre, O. S. Burren, S. P. Wilder, R. Kreuzhuber, S. M. Hill, S. Sewitz, J. Cairns, S. W. Wingett, C. Varnai, M. J. Thiecke, F. Burden, S. Farrow, A. J. Cutler, K. Rehnstrom, K. Downes, L. Grassi, M. Kostadima, P. Freire-Pritchett, F. Wang; BLUEPRINT Consortium, H. G. Stunnenberg, J. A. Todd, D. R. Zerbino, O. Stegle, W. H. Ouwehand, M. Frontini, C. Wallace, M. Spivakov, P. Fraser, Lineage-specific genome architecture links enhancers and non-coding disease variants to target gene promoters. *Cell* **167**, 1369–1384.e19 (2016).
9. M. R. Mumbach, A. T. Satpathy, E. A. Boyle, C. Dai, B. G. Gowen, S. W. Cho, M. L. Nguyen, A. J. Rubin, J. M. Granja, K. R. Kazane, Y. Wei, T. Nguyen, P. G. Greenside, M. R. Corces, J. Tycko, D. R. Simeonov, N. Suliman, R. Li, J. Xu, R. A. Flynn, A. Kundaje, P. A. Khavari, A. Marson, J. E. Corn, T. Quertermous, W. J. Greenleaf, H. Y. Chang, Enhancer connectome in primary human cells identifies target genes of disease-associated DNA elements. *Nat. Genet.* **49**, 1602–1612 (2017).
10. K. Monahan, A. Horta, S. Lomvardas, LHX2- and LDB1-mediated trans interactions regulate olfactory receptor choice. *Nature* **565**, 448–453 (2019).
11. F. Jin, Y. Li, J. R. Dixon, S. Selvaraj, Z. Ye, A. Y. Lee, C. A. Yen, A. D. Schmitt, C. A. Espinoza, B. Ren, A high-resolution map of the three-dimensional chromatin interactome in human cells. *Nature* **503**, 290–294 (2013).
12. S. Cruz-Molina, P. Respuela, C. Tebartz, P. Kolovos, M. Nikolic, R. Fueyo, W. F. J. van IJcken, F. Grosveld, P. Frommolt, H. Bazzi, A. Rada-Iglesias, PRC2 facilitates the regulatory topology required for poised enhancer function during pluripotent stem cell differentiation. *Cell Stem Cell* **20**, 689–705.e9 (2017).
13. F. Comoglio, H. J. Park, S. Schoenfelder, I. Barozzi, D. Bode, P. Fraser, A. R. Green, Thrombopoietin signaling to chromatin elicits rapid and pervasive epigenome remodeling within poised chromatin architectures. *Genome Res.* **28**, 295–309 (2018).
14. T. Fukaya, B. Lim, M. Levine, Enhancer control of transcriptional bursting. *Cell* **166**, 358–368 (2016).
15. W. Su, S. Jackson, R. Tjian, H. Echols, DNA looping between sites for transcriptional activation: Self-association of DNA-bound Sp1. *Genes Dev.* **5**, 820–826 (1991).
16. D. Campigli Di Giammartino, A. Kloetgen, A. Polyzos, Y. Liu, D. Kim, D. Murphy, A. Abuhashem, P. Cavaliere, B. Aronson, V. Shah, N. Dephoure, M. Stadtfeld, A. Tsirigos, E. Apostolou, KLF4 is involved in the organization and regulation of pluripotency-associated three-dimensional enhancer networks. *Nat. Cell Biol.* **21**, 1179–1190 (2019).
17. A. S. Weintraub, C. H. Li, A. V. Zamudio, A. A. Sigova, N. M. Hannett, D. S. Day, B. J. Abraham, M. A. Cohen, B. Nabet, D. L. Buckley, Y. E. Guo, D. Hnisz, R. Jaenisch, J. E. Bradner, N. S. Gray, R. A. Young, YY1 is a structural regulator of enhancer-promoter loops. *Cell* **171**, 1573–1588.e28 (2017).
18. S. Sakaguchi, T. Yamaguchi, T. Nomura, M. Ono, Regulatory T cells and immune tolerance. *Cell* **133**, 775–787 (2008).
19. S. Z. Josefowicz, L. F. Lu, A. Y. Rudensky, Regulatory T cells: Mechanisms of differentiation and function. *Annu. Rev. Immunol.* **30**, 531–564 (2012).
20. M. Panduro, C. Benoist, D. Mathis, Tissue Tregs. *Annu. Rev. Immunol.* **34**, 609–633 (2016).
21. A. R. Muñoz-Rojas, D. Mathis, Tissue regulatory T cells: Regulatory chameleons. *Nat. Rev. Immunol.* **21**, 597–611 (2021).
22. W. Lin, D. Haribhai, L. M. Relland, N. Truong, M. R. Carlson, C. B. Williams, T. A. Chatila, Regulatory T cell development in the absence of functional Foxp3. *Nat. Immunol.* **8**, 359–368 (2007).
23. M. A. Gavin, J. P. Rasmussen, J. D. Fontenot, V. Vasta, V. C. Manganiello, J. A. Beavo, A. Y. Rudensky, Foxp3-dependent programme of regulatory T-cell differentiation. *Nature* **445**, 771–775 (2007).
24. L. M. Charbonnier, Y. Cui, E. Stephen-Victor, H. Harb, D. Lopez, J. J. Bleesing, M. I. Garcia-Lloret, K. Chen, A. Ozen, P. Carmeliet, M. O. Li, M. Pellegrini, T. A. Chatila, Functional reprogramming of regulatory T cells in the absence of Foxp3. *Nat. Immunol.* **20**, 1208–1219 (2019).
25. D. Zemmour, L. M. Charbonnier, J. Leon, E. Six, S. Keles, M. Delville, M. Benamar, S. Baris, J. Zuber, K. Chen, B. Neven, M. I. Garcia-Lloret, F. M. Ruemmele, C. Brugnara, N. Cerf-Bensussan,

F. Rieux-Laucat, M. Cavazzana, I. Andre, T. A. Chatila, D. Mathis, C. Benoist, Single-cell analysis of FOXP3 deficiencies in humans and mice unmasks intrinsic and extrinsic CD4$^+$ T cell perturbations. *Nat. Immunol.* **22**, 607–619 (2021).
26. Y. Wu, M. Borde, V. Heissmeyer, M. Feuerer, A. D. Lapan, J. C. Stroud, D. L. Bates, L. Guo, A. Han, S. F. Ziegler, D. Mathis, C. Benoist, L. Chen, A. Rao, FOXP3 controls regulatory T cell function through cooperation with NFAT. *Cell* **126**, 375–387 (2006).
27. M. Ono, H. Yaguchi, N. Ohkura, I. Kitabayashi, Y. Nagamura, T. Nomura, Y. Miyachi, T. Tsukada, S. Sakaguchi, Foxp3 controls regulatory T-cell function by interacting with AML1/Runx1. *Nature* **446**, 685–689 (2007).
28. A. Kitoh, M. Ono, Y. Naoe, N. Ohkura, T. Yamaguchi, H. Yaguchi, I. Kitabayashi, T. Tsukada, T. Nomura, Y. Miyachi, I. Taniuchi, S. Sakaguchi, Indispensable role of the Runx1-Cbfβ transcription complex for in vivo-suppressive function of FoxP3$^+$ regulatory T cells. *Immunity* **31**, 609–620 (2009).
29. W. Fu, A. Ergun, T. Lu, J. A. Hill, S. Haxhinasto, M. S. Fassett, R. Gazit, S. Adoro, L. Glimcher, S. Chan, P. Kastner, D. Rossi, J. J. Collins, D. Mathis, C. Benoist, A multiply redundant genetic switch 'locks in' the transcriptional signature of regulatory T cells. *Nat. Immunol.* **13**, 972–980 (2012).
30. D. Rudra, P. Deroos, A. Chaudhry, R. E. Niec, A. Arvey, R. M. Samstein, C. Leslie, S. A. Shaffer, D. R. Goodlett, A. Y. Rudensky, Transcription factor Foxp3 and its protein partners form a complex regulatory network. *Nat. Immunol.* **13**, 1010–1019 (2012).
31. H. K. Kwon, H. M. Chen, D. Mathis, C. Benoist, Different molecular complexes that mediate transcriptional induction and repression by FoxP3. *Nat. Immunol.* **18**, 1238–1248 (2017).
32. R. M. Samstein, A. Arvey, S. Z. Josefowicz, X. Peng, A. Reynolds, R. Sandstrom, S. Neph, P. Sabo, J. M. Kim, W. Liao, M. O. Li, C. Leslie, J. A. Stamatoyannopoulos, A. Y. Rudensky, Foxp3 exploits a pre-existent enhancer landscape for regulatory T cell lineage specification. *Cell* **151**, 153–166 (2012).
33. H. Yoshida, C. A. Lareau, R. N. Ramirez, S. A. Rose, B. Maier, A. Wroblewska, F. Desland, A. Chudnovskiy, A. Mortha, C. Dominguez, J. Tellier, E. Kim, D. Dwyer, S. Shinton, T. Nabekura, Y. Qi, B. Yu, M. Robinette, K. W. Kim, A. Wagers, A. Rhoads, S. L. Nutt, B. D. Brown, S. Mostafavi, J. D. Buenrostro, C. Benoist; Immunological Genome Project, The cis-Regulatory atlas of the mouse immune system. *Cell* **176**, 897–912.e20 (2019).
34. L. A. Schubert, E. Jeffery, Y. Zhang, F. Ramsdell, S. F. Ziegler, Scurfin (FOXP3) acts as a repressor of transcription and regulates T cell activation. *J. Biol. Chem.* **276**, 37672–37679 (2001).
35. E. Bettelli, M. Dastrange, M. Oukka, Foxp3 interacts with nuclear factor of activated T cells and NF-kappa B to repress cytokine gene expression and effector functions of T helper cells. *Proc. Natl. Acad. Sci. U.S.A.* **102**, 5138–5143 (2005).
36. A. Arvey, J. van der Veeken, R. M. Samstein, Y. Feng, J. A. Stamatoyannopoulos, A. Rudensky, Inflammation-induced repression of chromatin bound by the transcription factor Foxp3 in regulatory T cells. *Nat. Immunol.* **15**, 580–587 (2014).
37. C. Chen, E. A. Rowell, R. M. Thomas, W. W. Hancock, A. D. Wells, Transcriptional regulation by Foxp3 is associated with direct promoter occupancy and modulation of histone acetylation. *J. Biol. Chem.* **281**, 36828–36834 (2006).
38. B. Li, A. Samanta, X. Song, K. T. Iacono, K. Bembas, R. Tao, S. Basu, J. L. Riley, W. W. Hancock, Y. Shen, S. J. Saouaf, M. I. Greene, FOXP3 interactions with histone acetyltransferase and class II histone deacetylases are required for repression. *Proc. Natl. Acad. Sci. U.S.A.* **104**, 4571–4576 (2007).
39. J. A. Hill, M. Feuerer, K. Tash, S. Haxhinasto, J. Perez, R. Melamed, D. Mathis, C. Benoist, Foxp3 transcription-factor-dependent and -independent regulation of the regulatory T cell transcriptional signature. *Immunity* **27**, 786–800 (2007).
40. A. Ferraro, A. M. D'Alise, T. Raj, N. Asinovski, R. Phillips, A. Ergun, J. M. Replogle, A. Bernier, L. Laffel, B. E. Stranger, P. L. De Jager, D. Mathis, C. Benoist, Interindividual variation in human T regulatory cells. *Proc. Natl. Acad. Sci. U.S.A.* **111**, E1111–E1120 (2014).
41. Y. Kitagawa, N. Ohkura, Y. Kidani, A. Vandenbon, K. Hirota, R. Kawakami, K. Yasuda, D. Motooka, S. Nakamura, M. Kondo, I. Taniuchi, T. Kohwi-Shigematsu, S. Sakaguchi, Guidance of regulatory T cell development by Satb1-dependent super-enhancer establishment. *Nat. Immunol.* **18**, 173–183 (2017).
42. I. Juric, M. Yu, A. Abnousi, R. Raviram, R. Fang, Y. Zhao, Y. Zhang, Y. Qiu, Y. Yang, Y. Li, B. Ren, M. Hu, MAPS: Model-based analysis of long-range chromatin interactions from PLAC-seq and HiChIP experiments. *PLoS Comput. Biol.* **15**, e1006982 (2019).
43. S. Bhattacharyya, V. Chandra, P. Vijayanand, F. Ay, Identification of significant chromatin contacts from HiChIP data by FitHiChIP. *Nat. Commun.* **10**, 4221 (2019).
44. F. A. Klein, T. Pakozdi, S. Anders, Y. Ghavi-Helm, E. E. Furlong, W. Huber, FourCSeq: Analysis of 4C sequencing data. *Bioinformatics* **31**, 3085–3091 (2015).
45. F. Grubert, R. Srivas, D. V. Spacek, M. Kasowski, M. Ruiz-Velasco, N. Sinnott-Armstrong, P. Greenside, A. Narasimha, Q. Liu, B. Geller, A. Sanghi, M. Kulik, S. Sa, M. Rabinovitch, A. Kundaje, S. Dalton, J. B. Zaugg, M. Snyder, Landscape of cohesin-mediated chromatin loops in the human genome. *Nature* **583**, 737–743 (2020).
46. H. K. Long, S. L. Prescott, J. Wysocka, Ever-changing landscapes: Transcriptional enhancers in development and evolution. *Cell* **167**, 1170–1187 (2016).
47. R. Siersbaek, J. G. S. Madsen, B. M. Javierre, R. Nielsen, E. K. Bagge, J. Cairns, S. W. Wingett, S. Traynor, M. Spivakov, P. Fraser, S. Mandrup, Dynamic rewiring of promoter-anchored chromatin loops during adipocyte differentiation. *Mol. Cell* **66**, 420–435.e5 (2017).
48. M. Song, M. P. Pebworth, X. Yang, A. Abnousi, C. Fan, J. Wen, J. D. Rosen, M. N. K. Choudhary, X. Cui, I. R. Jones, S. Bergenholtz, U. C. Eze, I. Juric, B. Li, L. Maliskova, J. Lee, W. Liu, A. A. Pollen, Y. Li, T. Wang, M. Hu, A. R. Kriegstein, Y. Shen, Cell-type-specific 3D epigenomes in the developing human cortex. *Nature* **587**, 644–649 (2020).
49. N. Sugimoto, T. Oida, K. Hirota, K. Nakamura, T. Nomura, T. Uchiyama, S. Sakaguchi, Foxp3-dependent and -independent molecules specific for CD25+CD4+ natural regulatory T cells revealed by DNA microarray analysis. *Int. Immunol.* **18**, 1197–1209 (2006).
50. J. A. Beagan, M. T. Duong, K. R. Titus, L. Zhou, Z. Cao, J. Ma, C. V. Lachanski, D. R. Gillis, J. E. Phillips-Cremins, YY1 and CTCF orchestrate a 3D chromatin looping switch during early neural lineage commitment. *Genome Res.* **27**, 1139–1152 (2017).
51. S. S. Hwang, S. W. Jang, M. K. Kim, L. K. Kim, B. S. Kim, H. S. Kim, K. Kim, W. Lee, R. A. Flavell, G. R. Lee, YY1 inhibits differentiation and function of regulatory T cells by blocking Foxp3 expression and activity. *Nat. Commun.* **7**, 10789 (2016).
52. J. van der Veeken, A. Glasner, Y. Zhong, W. Hu, Z. M. Wang, R. Bou-Puerto, L. M. Charbonnier, T. A. Chatila, C. S. Leslie, A. Y. Rudensky, The transcription factor Foxp3 shapes regulatory T cell identity by tuning the activity of trans-acting intermediaries. *Immunity* **53**, 971–984.e5 (2020).
53. R. N. Ramirez, K. Chowdhary, J. Leon, D. Mathis, C. Benoist, FoxP3 associates with enhancer-promoter loops to regulate Treg-specific gene expression. bioRxiv 468430. 17 November 2021; https://doi.org/10.1101/2021.11.12.468430.
54. E. Bettelli, Y. Carrier, W. Gao, T. Korn, T. B. Strom, M. Oukka, H. L. Weiner, V. K. Kuchroo, Reciprocal developmental pathways for the generation of pathogenic effector TH17 and regulatory T cells. *Nature* **441**, 235–238 (2006).
55. E. Lieberman-Aiden, N. L. van Berkum, L. Williams, M. Imakaev, T. Ragoczy, A. Telling, I. Amit, B. R. Lajoie, P. J. Sabo, M. O. Dorschner, R. Sandstrom, B. Bernstein, M. A. Bender, M. Groudine, A. Gnirke, J. Stamatoyannopoulos, L. A. Mirny, E. S. Lander, J. Dekker, Comprehensive mapping of long-range interactions reveals folding principles of the human genome. *Science* **326**, 289–293 (2009).
56. S. Ma, B. Zhang, L. M. LaFave, A. S. Earl, Z. Chiang, Y. Hu, J. Ding, A. Brack, V. K. Kartha, T. Tay, T. Law, C. Lareau, Y. C. Hsu, A. Regev, J. D. Buenrostro, Chromatin potential identified by shared single-cell profiling of RNA and chromatin. *Cell* **183**, 1103–1116.e20 (2020).
57. A. T. Satpathy, J. M. Granja, K. E. Yost, Y. Qi, F. Meschi, G. P. McDermott, B. N. Olsen, M. R. Mumbach, S. E. Pierce, M. R. Corces, P. Shah, J. C. Bell, D. Jhutty, C. M. Nemec, J. Wang, L. Wang, Y. Yin, P. G. Giresi, A. L. S. Chang, G. X. Y. Zheng, W. J. Greenleaf, H. Y. Chang, Massively parallel single-cell chromatin landscapes of human immune cell development and intratumoral T cell exhaustion. *Nat. Biotechnol.* **37**, 925–936 (2019).
58. J. D. Buenrostro, B. Wu, U. M. Litzenburger, D. Ruff, M. L. Gonzales, M. P. Snyder, H. Y. Chang, W. J. Greenleaf, Single-cell chromatin accessibility reveals principles of regulatory variation. *Nature* **523**, 486–490 (2015).
59. D. A. Cusanovich, A. J. Hill, D. Aghamirzaie, R. M. Daza, H. A. Pliner, J. B. Berletch, G. N. Filippova, X. Huang, L. Christiansen, W. S. DeWitt, C. Lee, S. G. Regalado, D. F. Read, F. J. Steemers, C. M. Disteche, C. Trapnell, J. Shendure, A single-cell atlas of in vivo mammalian chromatin accessibility. *Cell* **174**, 1309–1324.e18 (2018).
60. C. P. Fulco, J. Nasser, T. R. Jones, G. Munson, D. T. Bergman, V. Subramanian, S. R. Grossman, R. Anyoha, B. R. Doughty, T. A. Patwardhan, T. H. Nguyen, M. Kane, E. M. Perez, N. C. Durand, C. A. Lareau, E. K. Stamenova, E. L. Aiden, E. S. Lander, J. M. Engreitz, Activity-by-contact model of enhancer-promoter regulation from thousands of CRISPR perturbations. *Nat. Genet.* **51**, 1664–1669 (2019).
61. C. Buecker, J. Wysocka, Enhancers as information integration hubs in development: Lessons from genomics. *Trends Genet.* **28**, 276–284 (2012).
62. M. Lagha, J. P. Bothma, M. Levine, Mechanisms of transcriptional precision in animal development. *Trends Genet.* **28**, 409–416 (2012).
63. Y. Zheng, S. Z. Josefowicz, A. Kas, T. T. Chu, M. A. Gavin, A. Y. Rudensky, Genome-wide analysis of Foxp3 target genes in developing and mature regulatory T cells. *Nature* **445**, 936–940 (2007).
64. A. Marson, K. Kretschmer, G. M. Frampton, E. S. Jacobsen, J. K. Polansky, K. D. MacIsaac, S. S. Levine, E. Fraenkel, H. von Boehmer, R. A. Young, Foxp3 occupancy and regulation of key target genes during T-cell stimulation. *Nature* **445**, 931–935 (2007).
65. J. Zeitlinger, Seven myths of how transcription factors read the cis-regulatory code. *Curr. Opin. Syst. Biol.* **23**, 22–31 (2020).
66. V. K. Chaudhri, K. Dienger-Stambaugh, Z. Wu, M. Shrestha, H. Singh, Charting the cis-regulome of activated B cells by coupling structural and functional genomics. *Nat. Immunol.* **21**, 210–220 (2020).
67. A. Liston, K. M. Nutsch, A. G. Farr, J. M. Lund, J. P. Rasmussen, P. A. Koni, A. Y. Rudensky, Differentiation of regulatory Foxp3$^+$ T cells in the thymic cortex. *Proc. Natl. Acad. Sci. U.S.A.* **105**, 11903–11908 (2008).

68. B. Langmead, S. L. Salzberg, Fast gapped-read alignment with Bowtie 2. *Nat. Methods* **9**, 357–359 (2012).
69. F. Ramirez, D. P. Ryan, B. Gruning, V. Bhardwaj, F. Kilpert, A. S. Richter, S. Heyne, F. Dundar, T. Manke, deepTools2: A next generation web server for deep-sequencing data analysis. *Nucleic Acids Res.* **44**, W160–W165 (2016).
70. M. Lizio, I. Abugessaisa, S. Noguchi, A. Kondo, A. Hasegawa, C. C. Hon, M. de Hoon, J. Severin, S. Oki, Y. Hayashizaki, P. Carninci, T. Kasukawa, H. Kawaji, Update of the FANTOM web resource: Expansion to provide additional transcriptome atlases. *Nucleic Acids Res.* **47**, D752–D758 (2019).
71. T. Stuart, A. Srivastava, C. Lareau, R. Satija, Multimodal single-cell chromatin analysis with Signac. bioRxiv 373613. 10 November 2020. https://doi.org/10.1101/2020.11.09.373613.
72. J. M. Granja, M. R. Corces, S. E. Pierce, S. T. Bagdatli, H. Choudhry, H. Y. Chang, W. J. Greenleaf, ArchR: An integrative and scalable software package for single-cell chromatin accessibility analysis. bioRxiv 066498. 29 April 2020. https://doi.org/10.1101/2020.04.28.066498.
73. T. Stuart, A. Butler, P. Hoffman, C. Hafemeister, E. Papalexi, W. M. Mauck III, Y. Hao, M. Stoeckius, P. Smibert, R. Satija, Comprehensive integration of single-cell data. *Cell* **177**, 1888–1902.e21 (2019).
74. P. Shannon, A. Markiel, O. Ozier, N. S. Baliga, J. T. Wang, D. Ramage, N. Amin, B. Schwikowski, T. Ideker, Cytoscape: A software environment for integrated models of biomolecular interaction networks. *Genome Res.* **13**, 2498–2504 (2003).
75. N. Servant, N. Varoquaux, B. R. Lajoie, E. Viara, C. J. Chen, J. P. Vert, E. Heard, J. Dekker, E. Barillot, HiC-Pro: An optimized and flexible pipeline for Hi-C data processing. *Genome Biol.* **16**, 259 (2015).
76. J. Wolff, V. Bhardwaj, S. Nothjunge, G. Richard, G. Renschler, R. Gilsbach, T. Manke, R. Backofen, F. Ramirez, B. A. Gruning, Galaxy HiCExplorer: A web server for reproducible Hi-C data analysis, quality control and visualization. *Nucleic Acids Res.* **46**, W11–W16 (2018).
77. Y. Cao, S. Liu, G. Ren, Q. Tang, K. Zhao, cLoops2: A full-stack comprehensive analytical tool for chromatin interactions. bioRxiv 453068v1. 21 July 2021. https://doi.org/10.1101/2021.07.20.453068v1.
78. N. C. Durand, M. S. Shamim, I. Machol, S. S. Rao, M. H. Huntley, E. S. Lander, E. L. Aiden, Juicer provides a one-click system for analyzing loop-resolution Hi-C experiments. *Cell Syst.* **3**, 95–98 (2016).
79. D. Hnisz, B. J. Abraham, T. I. Lee, A. Lau, V. Saint-Andre, A. A. Sigova, H. A. Hoke, R. A. Young, Super-enhancers in the control of cell identity and disease. *Cell* **155**, 934–947 (2013).
80. C. A. Lareau, M. J. Aryee, diffloop: A computational framework for identifying and analyzing differential DNA loops from sequencing data. *Bioinformatics* **34**, 672–674 (2018).
81. Y. Zhou, B. Zhou, L. Pache, M. Chang, A. H. Khodabakhshi, O. Tanaseichuk, C. Benner, S. K. Chanda, Metascape provides a biologist-oriented resource for the analysis of systems-level datasets. *Nat. Commun.* **10**, 1523 (2019).
82. M. I. Love, W. Huber, S. Anders, Moderated estimation of fold change and dispersion for RNA-seq data with DESeq2. *Genome Biol.* **15**, 550 (2014).
83. M. Krzywinski, J. Schein, I. Birol, J. Connors, R. Gascoyne, D. Horsman, S. J. Jones, M. A. Marra, Circos: An information aesthetic for comparative genomics. *Genome Res.* **19**, 1639–1645 (2009).
84. C. A. Lareau, M. J. Aryee, hichipper: A preprocessing pipeline for calling DNA loops from HiChIP data. *Nat. Methods* **15**, 155–156 (2018).
85. D. H. Phanstiel, A. P. Boyle, N. Heidari, M. P. Snyder, Mango: A bias-correcting ChIA-PET analysis pipeline. *Bioinformatics* **31**, 3092–3098 (2015).
86. H. Wickham, *ggplot2: Elegant Graphics for Data Analysis* (Springer-Verlag, New York, 2009).
87. W. J. Kent, C. W. Sugnet, T. S. Furey, K. M. Roskin, T. H. Pringle, A. M. Zahler, D. Haussler, The human genome browser at UCSC. *Genome Res.* **12**, 996–1006 (2002).
88. J. T. Robinson, H. Thorvaldsdottir, W. Winckler, M. Guttman, E. S. Lander, G. Getz, J. P. Mesirov, Integrative genomics viewer. *Nat. Biotechnol.* **29**, 24–26 (2011).
89. R. N. Ramirez, K. Bedirian, S. M. Gray, A. Diallo, DNA Rchitect: An R based visualizer for network analysis of chromatin interaction data. *Bioinformatics* **36**, 644–646 (2020).

Acknowledgments: We thank C. Lareau, R. Young, and N. Ramirez for insightful discussions and K. Hattori, C. Araneo, K. Seddu, and the HMS Biopolymers team for help with mice, cell sorting, and sequencing. **Funding:** This work was funded by grants from the NIH to C.B. and D.M. (AI116834 and AI150686), J.L. was supported by an INSERM Poste d'Accueil and an Arthur Sachs scholarship, R.N.R. by NIH supplement AI116834-03S1, and K.C. by NIGMS-T32GM007753 and a Harvard Stem Cell Institute MD/PhD Training Fellowship. **Author contributions:** Conceptualization: R.N.R. and C.B. Investigation: R.N.R., K.C., and J.L. Supervision: C.B. Funding acquisition: C.B. and D.M. Writing—original draft: R.N.R., K.C., J.L., C.B., and D.M. Writing—review and editing: R.N.R. and C.B. **Competing interests:** The authors declare that they have no competing interests. **Data and materials availability:** Sequencing data can be found in the GEO database under accession number GSE190057. All data needed to evaluate the conclusions in the paper are present in the paper or the Supplementary Materials. All CBDM laboratory mice, including *Foxp3-327fs-gfp*, are freely available upon request from interested investigators.

Submitted 14 June 2021
Accepted 14 December 2021
Published 14 January 2022
10.1126/sciimmunol.abj9836

Science Immunology

FoxP3 associates with enhancer-promoter loops to regulate T-specific gene expression

Ricardo N. RamirezKaitavjeet ChowdharyJuliette LeonDiane MathisChristophe Benoist

Sci. Immunol., 7 (67), eabj9836.

Looping in FoxP3

The identity and function of T regulatory cells (T) relies on the activity of the transcription factor FoxP3, but its precise mechanism of action in controlling T-specific gene expression is not well understood. Using chromatin conformation capture with immunoprecipitation (HiChIP), Ramirez *et al.* mapped the enhancer-promoter architecture of conventional CD4 T cells and T and then identified FoxP3-interacting enhancer-promoter loops (EPLs). FoxP3 interacted with EPLs at core T signature genes and was associated with increased enhancer-promoter connectivity, while genetic inactivation of FoxP3 resulted in decreased H3K27Ac looping at the same loci. These results provide insight into FoxP3's interactions with EPLs and support a model in which FoxP3 directly regulates expression of many of its target genes through enhancer-promoter connections.

Science Immunology (ISSN) is published by the American Association for the Advancement of Science. 1200 New York Avenue NW, Washington, DC 20005. The title *Science Immunology* is a registered trademark of AAAS.